WRDC-TR-89-3031

COMPOSITE INTEGRITY MONITORING

Robert Rudd
Simmonds Precision
Instrument Systems Division
100 Panton Road
Vergennes, Vermont 05491

Kim Goddard
Hercules Aerospace Company
Aerospace Products Group
Bacchus Works
Magna, Utah 84044

May 1989

Final Report for Period September 1987 - August 1988

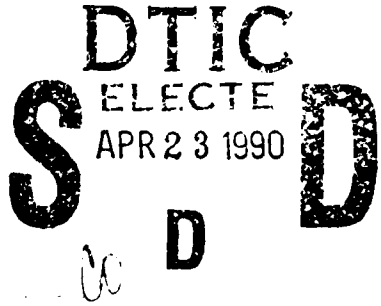

FLIGHT DYNAMICS LABORATORY
WRIGHT RESEARCH AND DEVELOPMENT CENTER
AIR FORCE SYSTEMS COMMAND
WRIGHT-PATTERSON AIR FORCE BASE, OHIO 45433-6553

NOTICE

When Government drawings, specifications, or other data are used for any purpose other than in connection with a definitely Government-related procurement, the United States Government incurs no responsibility or any obligation whatsoever. The fact that the government may have formulated or in any way supplied the said drawings, specifications, or other data, is not to be regarded by implication, or otherwise in any manner construed, as licensing the holder, or any other person or corporation; or as conveying any rights or permission to manufacture, use, or sell any patented invention that may in any way be related thereto.

This report is releasable to the National Technical Information Service (NTIS). At NTIS, it will be available to the general public, including foreign nations.

This technical report has been reviewed and is approved for publication.

George P. Sendeckyj

GEORGE P. SENDECKYJ
Project Engineer
Fatigue, Fracture & Reliability Group

James L. Rudd

JAMES L. RUDD, Tech Mgr
Fatigue, Fracture & Reliabilty Group
Structural Integrity Branch

FOR THE COMMANDER

George E Muller

GEORGE E. MULLER, Chief
Structural Integrity Branch

If your address has changed, if you wish to be removed from our mailing list, or if the addressee is no longer employed by your organization please notify WRDC/FIBEC, WPAFB, OH 45433-6553 to help us maintain a current mailing list.

Copies of this report should not be returned unless return is required by security considerations, contractual obligations, or notice on a specific document.

SECURITY CLASSIFICATION OF THIS PAGE

REPORT DOCUMENTATION PAGE

Form Approved
OMB No. 0704-0188

1a. REPORT SECURITY CLASSIFICATION UNCLASSIFIED	1b. RESTRICTIVE MARKINGS NONE
2a. SECURITY CLASSIFICATION AUTHORITY N/A	3. DISTRIBUTION/AVAILABILITY OF REPORT Approved for Public Release, distribution unlimited.
2b. DECLASSIFICATION/DOWNGRADING SCHEDULE N/A	
4. PERFORMING ORGANIZATION REPORT NUMBER(S)	5. MONITORING ORGANIZATION REPORT NUMBER(S) WRDC-TR-89-3031
6a. NAME OF PERFORMING ORGANIZATION Simmonds Precision Instrument Systems Division 6b. OFFICE SYMBOL (If applicable)	7a. NAME OF MONITORING ORGANIZATION Wright Research and Development Center Flight Dynamics Laboratory (WRDC/FIBEC)
6c. ADDRESS (City, State, and ZIP Code) Vergennes, Vermont 05491	7b. ADDRESS (City, State, and ZIP Code) W-PAFB OH 45433-6553
8a. NAME OF FUNDING/SPONSORING ORGANIZATION 8b. OFFICE SYMBOL (If applicable) FIBEC	9. PROCUREMENT INSTRUMENT IDENTIFICATION NUMBER F33615-87-C-3241
8c. ADDRESS (City, State, and ZIP Code)	10. SOURCE OF FUNDING NUMBERS PROGRAM ELEMENT NO. 61101F; PROJECT NO. 2401; TASK NO. 07; WORK UNIT ACCESSION NO. 09
11. TITLE (Include Security Classification) Composite Integrity Monitoring	
12. PERSONAL AUTHOR(S) R. Rudd and K. Goddard	
13a. TYPE OF REPORT Final	13b TIME COVERED FROM Sep 87 TO Aug 88
14 DATE OF REPORT (Year, Month, Day) 1989 May	15 PAGE COUNT 79
16. SUPPLEMENTARY NOTATION	

17. COSATI CODES		
FIELD	GROUP	SUB-GROUP
11	04	
01	03	

18. SUBJECT TERMS (Continue on reverse if necessary and identify by block number)
Composite Material, Fiber Optics, Strain Measurement, Structural Integrity Monitoring

19. ABSTRACT (Continue on reverse if necessary and identify by block number)

Optical fibers were embedded in graphite epoxy composite coupons and I-beams with the objective of measuring integrated and distributed loads. Polarimetric techniques using both high and low birefringence optical fibers were used for integrated strain, while optical time domain reflectometry (OTDR) was used for locating distributed point loads. Polarimetric results agreed favorably with resistence strain gage data when the structure app'ied load normal to the optical fiber axis. Stresses of 64 ksi were required to observe loads using OTDR with a resolution of 1.2 meters.

20. DISTRIBUTION/AVAILABILITY OF ABSTRACT ☒ UNCLASSIFIED/UNLIMITED ☐ SAME AS RPT. ☐ DTIC USERS	21. ABSTRACT SECURITY CLASSIFICATION UNCLASSIFIED
22a NAME OF RESPONSIBLE INDIVIDUAL George P. Sendeckyj	22b. TELEPHONE (Include Area Code) (513) 255-6104 22c OFFICE SYMBOL WRDC/FIBEC

DD Form 1473, JUN 86 *Previous editions are obsolete.* SECURITY CLASSIFICATION OF THIS PAGE

REPORT SUMMARY

Optical fibers were embedded in graphite epoxy composite coupons and I-beams with the objective of measuring integrated and distributed loads. Polarimetric techniques using both high and low birefringent optical fibers were used for integrated strain while Optical Time Domain Reflectometry was used for locating distributed point loads.

Eighteen uniaxial graphite epoxy coupons were manufactured during Preliminary Fabrication and Testing. Fiber optic sensors were embedded at different orientations with respect to the graphite fibers and the coupon neutral axis. Strain applied normal to the axis of a low birefringence optical fiber produced an optical signal which correlated well with a resistive strain gage. Strain applied along the axis of a high birefringence optical fiber produced an optical signal which did not correlate well with a resistive strain gage. Theoretical and experimental results were developed which show high birefringence fiber to be more sensitive to loading normal to the optic axis than parallel. Furthermore, laser diode wavelength stability was shown to complicate strain measurement for the high birefringence fiber.

Optical Time Domain Reflectometry (OTDR) was used to locate point loads applied to test coupons. System resolution was shown to be on the order of 1.2 meters. Point loads became apparent at about 64,000 psi compressive stress normal to the optical and graphite fibers. Since this load is near the compressive strength of the composite, OTDR was recommended for damage detection.

Two composite I-beams were fabricated with polarimetric low birefringence optical fiber sensors embedded in the flange perpendicular to length. The beam was loaded in four point bending. Optical and resistive strain measurements correlated well.

Optical fiber survival rate was fifty percent during composite fabrication. Survivability was compromised by removal of the optical fibers acrylate buffer to obtain improved mechanical load transfer to the optical fiber. Gold coated fibers were embedded in an effort to obtain good survival and load transfer; however, the gold fiber survival rate was no better than the unbuffered fiber. The gold coated fiber exhibited hysteresis not present in bare fiber tests.

TABLE OF CONTENTS

		Page No.
	SUMMARY	iii
	TABLE OF CONTENTS	iv
	LIST OF FIGURES	v
	LIST OF TABLES	vii
1.0	INTRODUCTION	1
	1.1 Technology Review	2
2.0	PRELIMINARY FABRICATION AND TESTING	10
	2.1 Coupon Fabrication	12
	2.2 Instrumentation Verification	12
	2.3 Coupon Four Point Bend Test	24
	2.4 Coupon Compression Testing	24
	2.5 Coupon Stress to Failure	25
	2.6 Coupon Test Analysis	29
	2.7 OTDR Testing	41
3.0	I-BEAM STRUCTURAL FABRICATION AND TESTING	48
	3.1 I-Beam Design	48
	3.2 I-Beam Fabrication	48
	3.3 I-Beam Four Point Bend Test	53
	3.4 I-Beam Load to Failure Test	61
	3.5 I-Beam Test Analysis	64
4.0	CONCLUSIONS	67
5.0	RECOMMENDATIONS	68
	REFERENCES	69
	APPENDICES	70
	A. Statement of Work	70

LIST OF FIGURES

Figure No.		Page No.
1	Photoelastic Effect	4
2	Low Birefringence Optical Fiber and Normal Load	5
3	High Birefringence Optical Fiber and Axial Load	7
4	Optical Time Domain Reflectometry	9
5	Coupon Configuration	11
6	Polarimetric Instrumentation Verification Coupon Loading	14
7	Polarimetric Instrumentation Photograph	16
8	Polarimetric Instrumentation Verification Data Plot	19
9	Coupon Tensile Test Data Plot	25
10	Grip Pressurization Data Plot	28
11	Optical Fiber Loading Models	33
12	Four Point Bend Strain Distribution	40
13	Initial OTDR Test Schematic	42
14	OTDR Resolution Test Traces	43
15	Revised OTDR Test Schematic	44
16	Revised OTDR Test Traces	45
17	I-Beam Dimensions	49
18	I-Beam Lay Up	50

LIST OF FIGURES

Figure No.		Page No.
19	Fully Instrumented I-Beam Photograph	51
20	I-Beam Four Point Loading Fixture Photograph	54
21	I-Beam Measurement Equipment Photograph	55
22	I-Beam Data Plot	56
23	I-Beam Reduced Data Plot	58
24	Gold Fiber Data Plot	59
25	Gold Fiber Reduced Data Plot	60
26	Failed I-Beam	62

LIST OF TABLES

Table No.		Page No.
1	Optical Fiber Survival by Coupon Type	13
2	Optical Fiber Survival by Optical Fiber Type	15
3	Polarization Measurements	18
4	Polarimetric Data Reduction	21
5	Instrument Verification Optical Responsivity	22
6	Four Point Bend Test Coupon Optical Responsivity	26
7	Coupon Failure Test Results - Tension	30
8	Coupon Failure Test Results - Compression	31
9	Theoretical and Empirical Comparison of Transverse Strain Responsivity	38
10	I-Beam Optical Fiber Survival Rate	52
11	I-Beam Optical Responsivity Results	57
12	Predicted Versus Actual I-Beam Failure Load	63
13	I-Beam Fiber Optical Responsivity Results	66

1.0 INTRODUCTION

Present and future aircraft, missiles and space vehicles are increasing the use of graphite epoxies in their construction. These new materials are lighter (30% less weight than aluminum) and stronger, as well as being less susceptible to radar detection and allow more flexibility in the design and fabrication that is necessary to meet performance requirements of future aircraft.

Hercules Inc., and its subsidiary Simmonds Precision are addressing these new aircraft and space vehicles by developing new sensors, actuators and processors that can be integrated into the composite skin and structure that will provide them with intelligence and control.

This contract is addressing the measurement of strain within the composite. The approach taken was to characterize embedded fiber optic sensors in relatively simple structures. Fiber sensor types chosen for investigation were:

- Polarimetric
- Optical Time Domain Reflectometry (OTDR).

Structure types chosen were:

- Unidirectional Composite Coupons (10" x 1.5" x 24 plies)
- Composite I-beam (15.0" x 1" x 1.23").

Load conditions for the composite coupons were:

- Four Point Bending
- 0° Compression.

Load condition for the I-beam was four point bending.

1.1 Technology Review

Two optical configurations were chosen for investigation.

- Polarimetric
- Optical Time Domain Reflectometry (OTDR)

A Polarimetric system monitors the State of Polarization (SOP) of the light emerging from the sensor. Load applied to the fiber changes the emerging SOP. An OTDR system monitors the light back scattering from a forward propagating optical pulse. Load applied to the fiber changes the amount of back scattered light. Descriptions of the physical mechanisms are given below.

Polarimetric Technique

The Polarimetric technique uses two types of optical fiber sensors

- Low Birefringence Fiber - transverse load
- High Birefringence Fiber - axial load

Low birefringence fiber is used to measure loads applied transversely to the optic fiber axis. High birefringence fiber is used to measure loads applied along the optical axis. Birefringence is a term used to describe the index of refraction of the glass in the optical fiber. If light polarized in the X direction travels at the same speed as light polarized in the Y direction, the fiber has zero birefringence. In practice, irregularities in the material and geometric properties of the optical fiber make zero birefringence impossible. Optical fibers which are nominally zero birefringence are referred to as low birefringence for the remainder of this report.

High birefringence optical fibers have differing indices of refraction in the X and Y direction. An anisotropy upsets the symmetry of the refractive index profile in the fiber core region[1]. High birefringence fiber described in this report has stress induced material anisotropy.

The photoelastic effect, illustrated in Figure 1, is the mechanism by which strain is measured in the polarimetric technique. Linearly polarized light, resolved into equal amplitude in the X and Y direction is shown entering a photoelastic material. Strain applied normal to the light path causes a change in the X and Y index of refraction. In the situation shown, the horizontal component is

moving slower and a spatial (or time) delay is created. A spatial delay of one quarter of a wavelength is shown. This is called circularly polarized light as this is the shape the electric field vector traces out when viewed along the optic axis.

If a second compressive strain of equal magnitude is introduced perpendicular to the first, the vertical component will be retarded equal to the horizontal component and no relative difference will be observed. The photoelastic effect is therefore insensitive to hydrostatic loading. The spatial delay is usually referenced to the optical wavelength in use and reported as a phase difference. Care must be taken when using phase difference however. For example, if the optical wavelength is halved the phase difference is doubled for an identical spatial delay. (Most of the work discussed in this report used 820 nm optical wavelength however 632 nm was used at times.) Also note that if the length of photoelastic material under strain doubles, the spatial delay doubles.

The polarimetric technique does not give an absolute measurement. If a strain is applied to the fiber while the system is off, undetectable strain will occur. Ambiguity occurs due to the cyclic nature of the signal. One cycle of retardation cannot be distinguished from another without tracking from zero load.

Low Birefringence Fiber

The photoelastic effect internal to a low birefringence optical fiber under load normal to its axis is shown in Figure 2. An optical fiber loaded along its length creates a stress difference and hence an index of refraction difference in the fiber core. When circularly polarized light (which has no angular preference) is launched into an unloaded optical fiber, the light propagates unchanged as illustrated in Figure 2. When loaded, the polarization evolves from circular to elliptical to linear, etc. One complete cycle of polarization evolution is equivalent to a spatial delay of one wavelength.

Units used to describe the strain response in this report are fringes per % strain per inch and is referred to as optical responsivity. A fringe is equivalent to a spatial delay of one wavelength and is used because of its uniqueness. Describing the delay in other units such as radians, degrees, revolutions, cycles, wavelengths, time or distance can sometimes cause confusion with other quantities involved. Fringes are normalized with respect to % strain

TRANSVERSE STRAIN-STRESS INDUCED BIREFRINGENCE

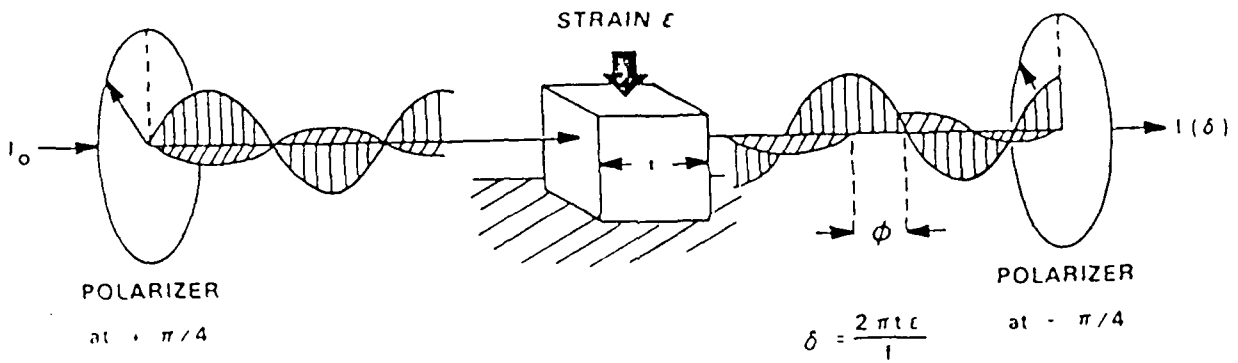

FIGURE 1. PHOTOELASTIC EFFECT

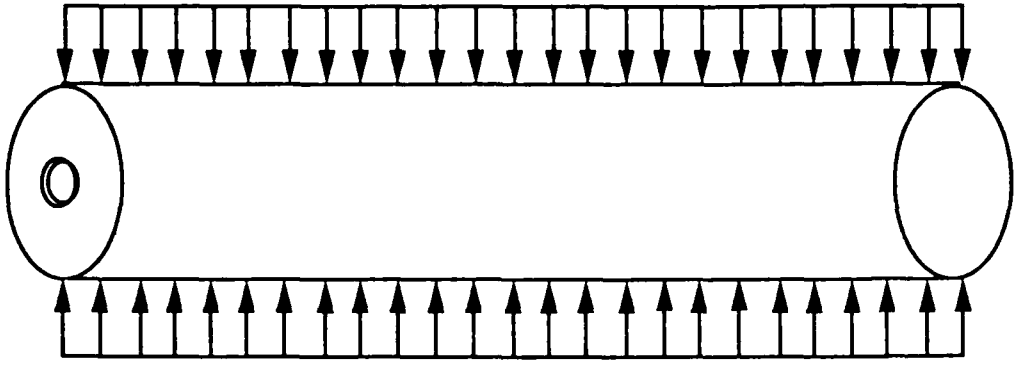

POLARIZATION STATE EVOLUTION

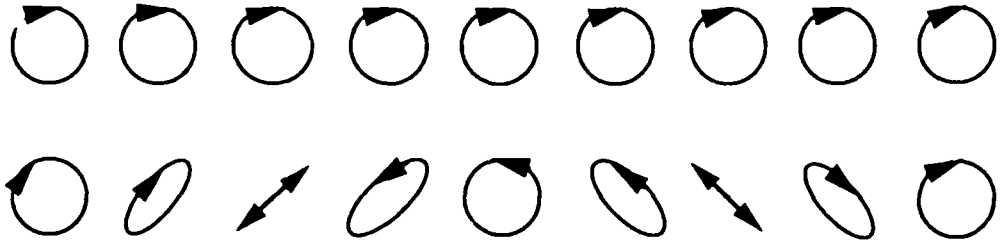

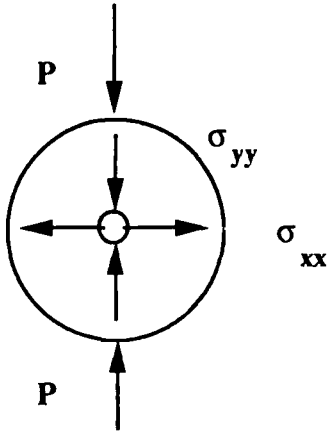

$\Delta\Phi_t \propto \sigma_{yy} - \sigma_{xx}$

No Transverse Strain

Transverse Strain

FIGURE 2. LOW BIREFRINGENCE : OPTICAL FIBER AND NORMAL LOAD

and inches. Normalization with respect to length allows comparison of results where different (gage) lengths of optical fiber are loaded. (If length of fiber being strained doubles, the amount of spatial delay doubles.) Optical responsivity is equivalent to the gage factor in a resistive strain gage.

High Birefringence Fiber

High birefringence fiber, in its unloaded state, has strain applied normal to the fiber core. "Stress lobes" are built into the optical fiber preform before drawing down to the fiber diameter. The stress lobes, shown schematically in Figure 3, have elastic and thermal properties differing from the surrounding core material. Upon cooling, differential thermal contraction loads the fiber core and an intrinsic birefringence occurs in the core.

When circularly polarized light is launched into an unloaded high birefringence optical fiber, the SOP evolves from circular to elliptical to linear, etc. One complete cycle of polarization evolution is equivalent to a relative spatial delay of one wavelength. The length of fiber which is required for SOP cycles to occur is called the beat length. High birefringence fiber discussed in this report was specified by the manufacturer as 2 mm beat length.

Strain applied along the fiber core causes two effects to occur which are illustrated in Figure 3. The fiber is physically lengthened so the light has a longer path over which to evolve. Differential Poisson's contraction, due to directional elastic properties, cause further transverse loading of the fiber core. The beat length is further decreased.

The unit used to describe the axial strain response also is fringes per % strain per length. This unit is somewhat redundant as the length in the strain term and fiber length are one and the same and would cancel. The length is carried along for consistency with the low birefringence fiber optical responsivity.

Optical Time Domain Reflectometry

An OTDR system is depicted in Figure 4. An optical source is driven to create a pulse of light. The pulse passes through a beam splitter and is launched into an optical fiber. A small portion of the forward propagating pulse is continuously back scattered. Back scattered light emerges from

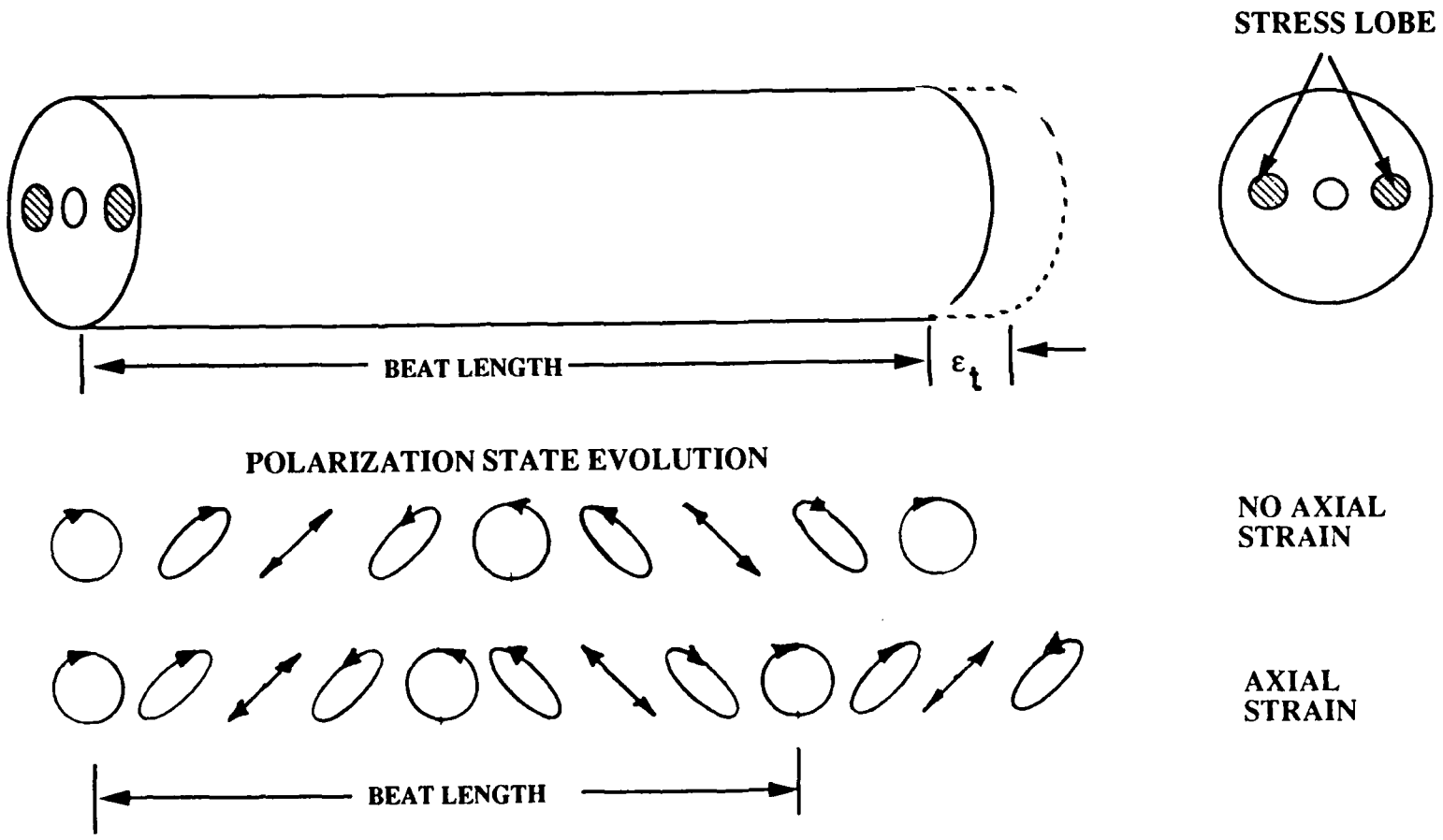

FIGURE 3. HIGH BIREFRINGENCE OPTICAL FIBER AND AXIAL LOAD

the optical fiber where a beam splitter directs the light to a photodetector. Under normal conditions the photodetector produces an exponentially decaying signal versus time. The signal logarithm is a straight line representing normal attenuation in the fiber. Time is related to distance along the optical fiber via the speed of light in the fiber.

A perturbation in the optical fiber via point loading produces a step loss of forward and backward propagating light (via microbending). The location of the point load can be determined by position of the step loss in the signal logarithm data.

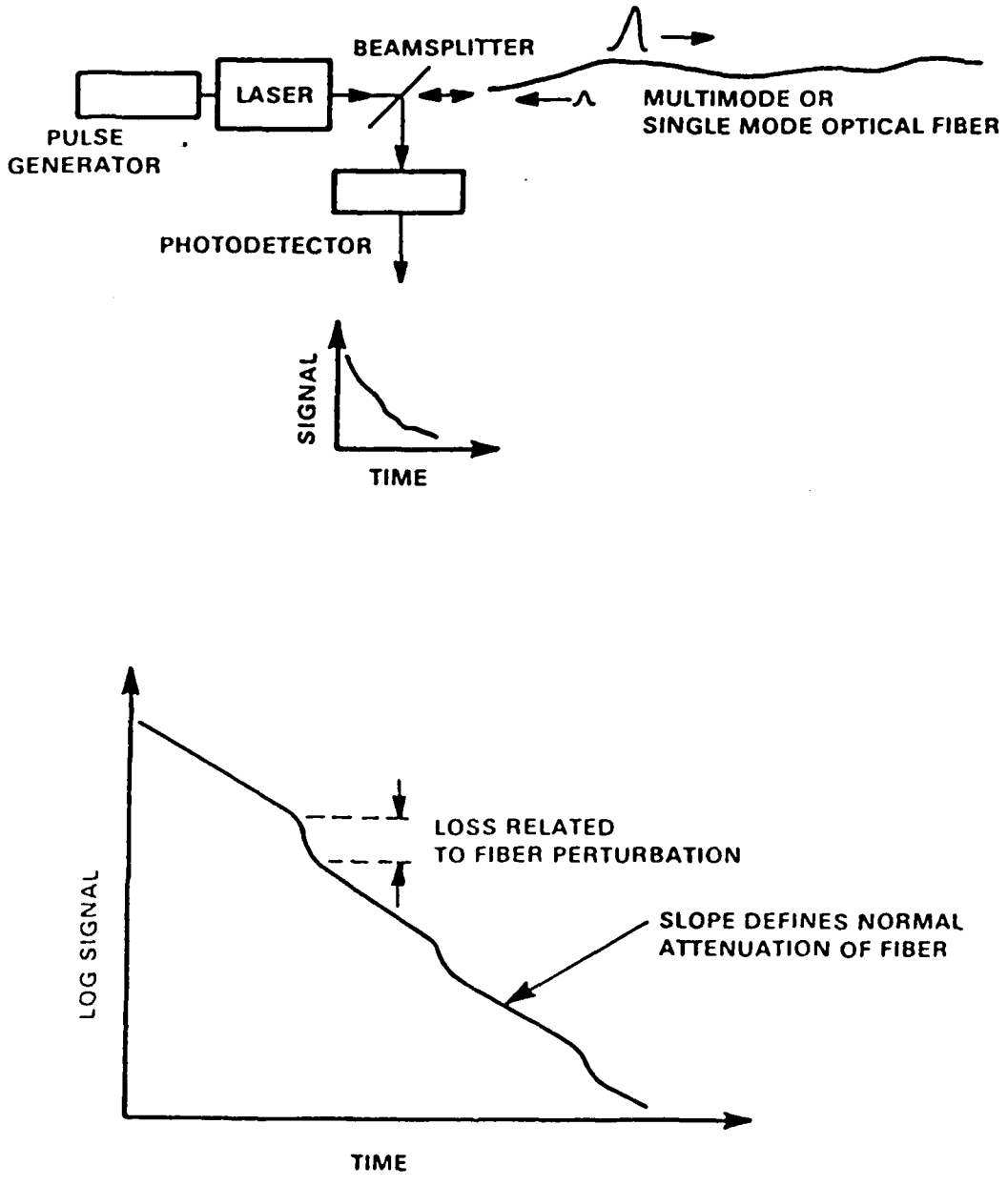

FIGURE 4. OPTICAL TIME DOMAIN REFLECTOMETRY

2.0 PRELIMINARY FABRICATION AND TESTING

This section describes fabrication and testing of 0° graphite epoxy coupons with and without embedded optical fibers. Appendix 1 contains the Statement of Work. Fiber optic sensors described previously were embedded in the coupon at various orientations with respect to applied loads and the graphite fibers. Figure 5 illustrates coupon configurations. All coupons were 1.5 inches wide by 24 plies thick. Coupon lengths were either 6 or 10 inches. Material was Hercules AS4/3501-6. Three coupons in each of the six configurations were fabricated. Coupons were unidirectional.

Configuration "A" coupons were loaded in four point bending and have optical fiber sensor embedded along the center. The outer two fibers were multimode 50/125 micron optical fiber for OTDR. Low birefringence single mode (820 nm) optical fibers reside next to the multimode fibers. The center fiber was a high birefringence single mode (820 nm) optical fiber with a 2 mm beat length. Duplicate fibers were embedded to provide a level of protection against breakage. High birefringence fiber was not duplicated.

Configuration "B" coupons were the same as "A" coupons except the fibers were moved to a plane halfway between the center and surface. For both "A" and "B" coupons the load rollers provided transverse loading to the optical fibers for the polarimetric technique as well as a point load for OTDR. Furthermore, by placing the optical fiber off center, axial loading was applied to the high birefringence fiber.

Configuration "C" coupons had optical fibers embedded at 90° to the 0° graphite fibers. Multimode fibers were not embedded since the point load condition would not be applied in four point bend. Four point bending would apply transverse loading to the optical fiber for use with transverse loading.

Configuration "D" coupons were similar to configuration "C" coupons except the coupon was shorter (6" vs. 10") and the multimode fibers were omitted. Configuration "D" coupons were loaded in 0° direction.

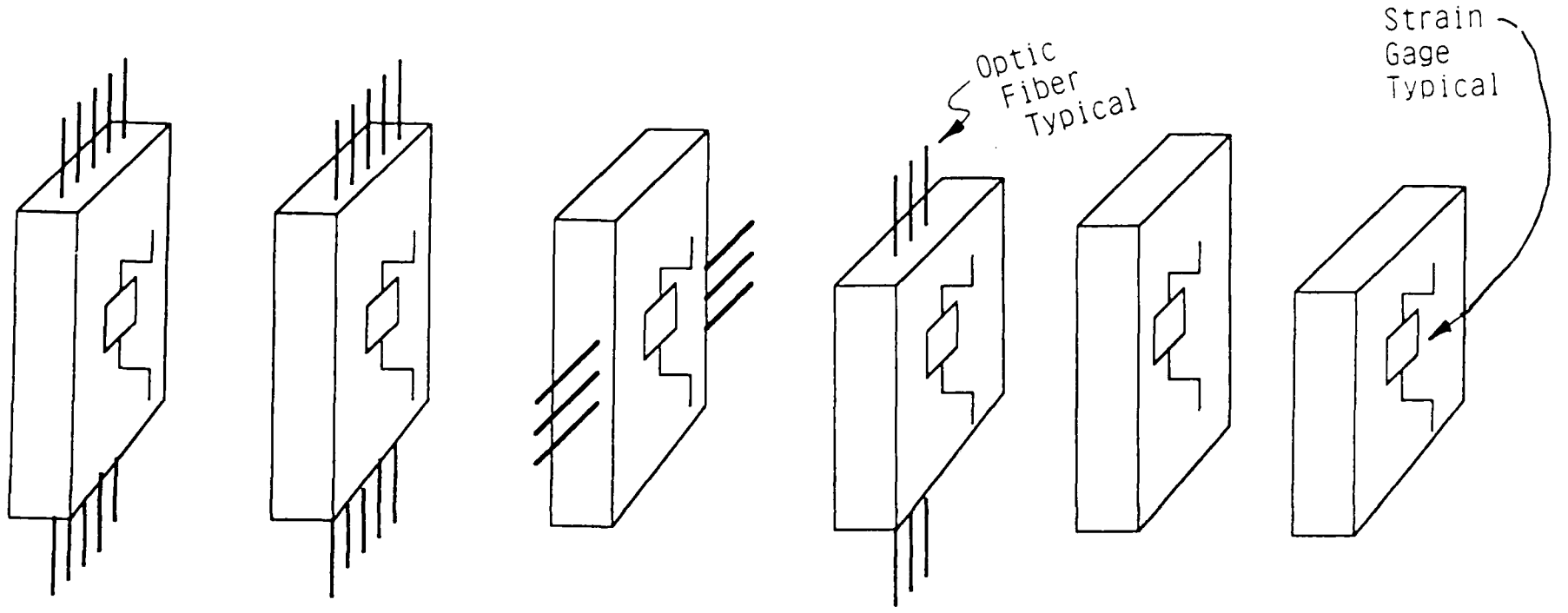

Tensile Coupons	10" X 1 1/2" X 24 0° Plys
Compressive Coupons	6" X 1 1/2" X 24 0° Plys

FIGURE 5. COUPON CONFIGURATION

Configuration "E" and "F" coupons are control specimens for "A", "B", "C" and "D" coupons respectively. All coupons are to be loaded to failure (A, B, C, E in tension, D, F in compression) to determine the effect of embedded optical fibers on ultimate strength.

Low and high birefringence optical fiber had the acrylate coating removed to improve load transfer to the optical fiber. Previous results [2] showed hysteresis was associated with the buffer material. Multimode fiber was embedded with the acrylate buffer intact to ease handling and minimize fiber breakage potential.

One biaxial strain gage was attached on the surface at the center of each coupon. When the optical fiber was located off center, the strain gage was attached on the side closest to the optical fibers.

2.1 Coupon Fabrication

Coupons were fabricated as described in section 2.0. Optical fiber survival rate was approximately 50%. Since all high birefringence optical fibers in the "B" coupons were damaged, an additional "B" coupon was fabricated with three high birefringence fibers. Survival was determined by measuring optical throughput with 1200 microwatt HeNe laser as input. Throughput was clearly bimodal with broken fibers measuring less than 5 microwatts output and continuous fibers measuring between 180 and 1100 microwatts. Fiber survival is tabulated by coupon type in Table 1 and fiber type in Table 2. Multimode fiber embedded with the acrylate coating intact had the highest survival rate.

2.2 Polarimetric Instrumentation Verification

Prior to performing testing described in Section 2.0, one coupon was loaded in uniaxial tension as shown in Figure 6. The purpose of this additional testing was to verify proper operation of the polarimetric instrumentation in a known configuration. Coupon "C" #3, used as this coupon, had optically continuous low and high birefringence optical fibers loaded with a transverse strain.

Figure 7 shows the polarimetric optical equipment. An 820 nm laser diode is located to the far left. Light emerging from the laser passes through a polarizer with its transmission axis mounted horizontal. A quarter waveplate with its first axis at 45° to horizontal transforms the linear polarized light to circular before launch into the optical fiber. Circularly polarized light has

TABLE 1. OPTICAL FIBER SURVIVAL BY COUPON TYPE

COUPON TYPE	COUPON #	FIBER # MULTIMODE #1	LOW BI #1	HIGH BI	LOW BI #2	MULTIMODE #2
A	1	P	F	P	F	F
	2	P	F	F	F	F
	3	P	F	F	F	F
B	1	P	F	F	P	P
	2	P	P	F	F	P
	3	P	F	F	F	P
	4*	-	-	P/P/P	-	-
C	1	-	F	P	P	-
	2	-	F	P	F	-
	3	-	F	P	P	-
D	1	-	F	F	F	-
	2	-	F	P	F	-
	3	-	F	F	P	-

P = Passed Optical Continuity Test

F = Failed Optical Continuity Test

* ADDITIONAL COUPON WITH THREE HIGH BIREFRINGENCE FIBERS

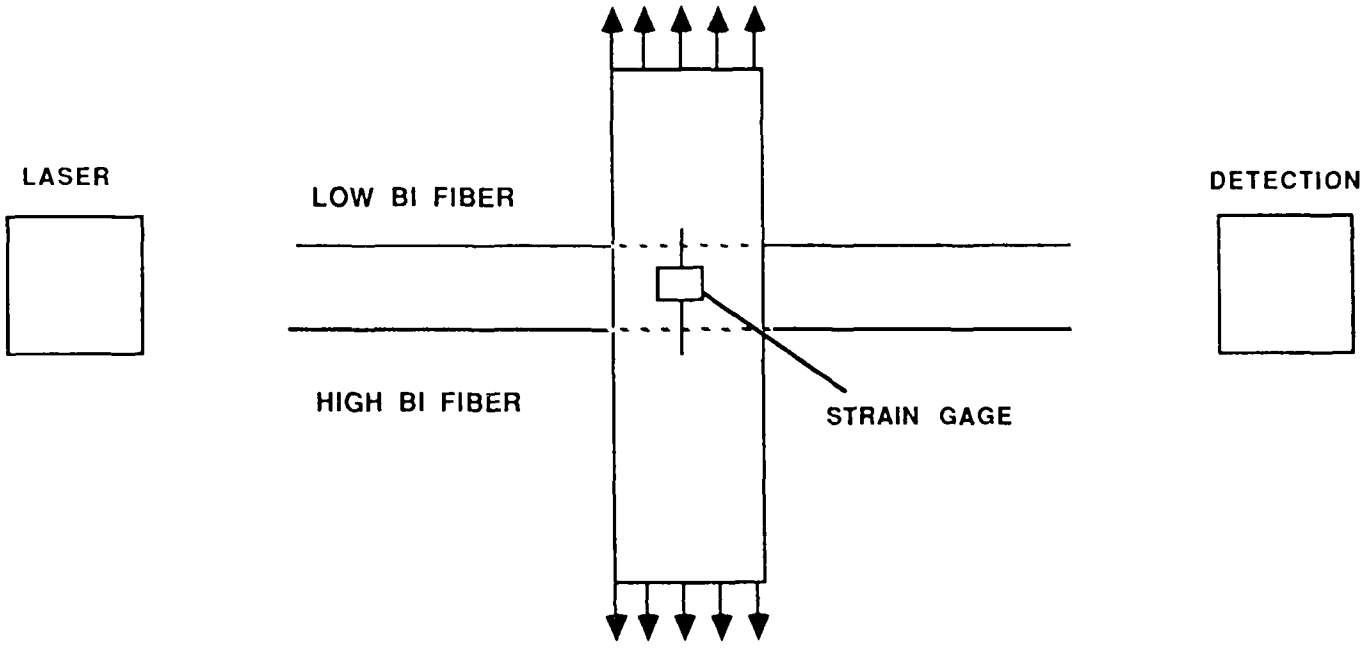

FIGURE 6. POLARIMETRIC INSTRUMENTATION VERIFICATION COUPON LOADING

TABLE 2. OPTICAL FIBER SURVIVAL BY OPTICAL FIBER TYPE

OPTICAL FIBER TYPE	BUFFER	# EMBEDDED	# SURVIVED	SURVIVAL RATE
MULTIMODE	YES	12	9	75%
LOW BIREFRINGENCE	NO	24	5	21%
HIGH BIREFRINGENCE	NO	15	8	53%
TOTAL	51	22	43%	

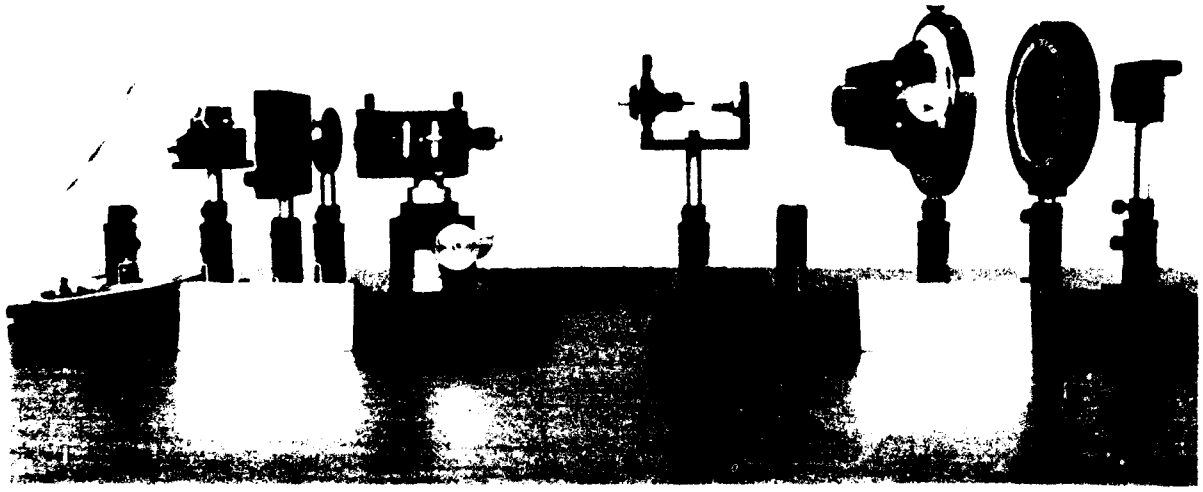

FIGURE 7. POLARIMETRIC INSTRUMENTATION PHOTOGRAPH

no preferred angular orientation. Coupling to high birefringence fiber, which has a definite axis, is made easier as relative angular orientation is removed as a variable.

Laser diode optical output is electrically stabilized to 7.00 milliwatts. Stabilization occurs via feeding the laser diode monitor beam to a photodetector and comparing photodetector output to 7.00 milliwatts. Laser diode drive current is then electrically adjusted to drive the difference to zero. Feedback loop stability is $\pm$ 10 microwatts and bandwidth is approximately 5 KHz.

Optical power entering the optical fiber is not measured.

Receive optics are shown on the right hand side of Figure 7. Light is collimated by a positioning device and .1 numerical aperture microscope objective. A Soliel-Babinet (SB) compensator is the next element in the optical path. An SB compensator introduces a variable retardation into the optical path. The compensator is set with its fast axis horizontal with a quarter wave retardation. A polarizer and photodetector follow. The polarizer may be moved to a stand between the SB compensator and microscope objective; in which case, the SB compensator performs no function (the photo detector is polarization insensitive).

Six measurements can be made with the equipment as configured and they are tabulated in Table 3. The six measurements are advantageous in that

$$S_1 = \frac{I_1 - I_2}{I_1 + I_2} \qquad (2.2\text{-}1)$$

$$S_2 = \frac{I_3 - I_4}{I_3 + I_4} \qquad (2.2\text{-}2)$$

$$S_3 = \frac{I_5 - I_6}{I_5 + I_6} \qquad (2.2\text{-}3)$$

where I_i (i = 1, 2, ... 6) represents the six photodetector signals and S_i (i = 1, 2, 3) are components of the Stokes vector. The Stokes vector is a method of describing the state of polarization of optical energy and can be related to strain induced birefringences [3]. Further benefits are that the difference over sum operation desensitizes the system to bias (photodetector dark current for example) and scaling (power level for example).

TABLE 3. POLARIZATION MEASUREMENTS

MEASUREMENT #	MNEMONIC	OPTICAL CONFIGURATION 0° = HORIZONTAL
1	I_1	Polarizer @ 0°
2	I_2	Polarizer @ 90°
3	I_3	Polarizer @ +45°
4	I_4	Polarizer @ -45°
5	I_5	Quarterwave plate @ 0°, Polarizer @ 45°
6	I_6	Quarterwave plate @ 0°, Polarizer @ -45°

AXIAL STRAIN GAGE OUTPUT (ELECTRICAL)

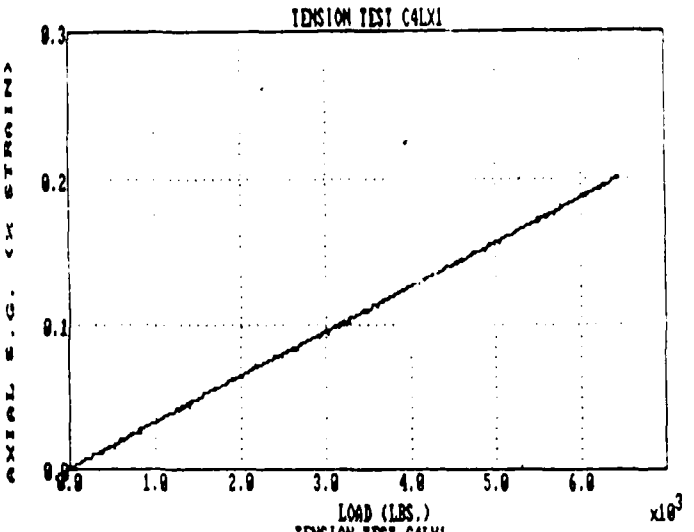

LOW BIREFRINGENCE FIBER OUTPUT (OPTICAL)

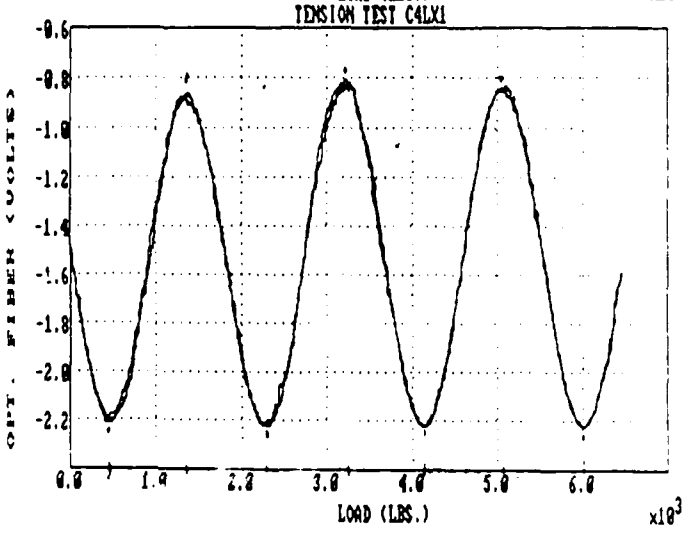

HIGH BIREFRINGENCE FIBER OUTPUT (OPTICAL)

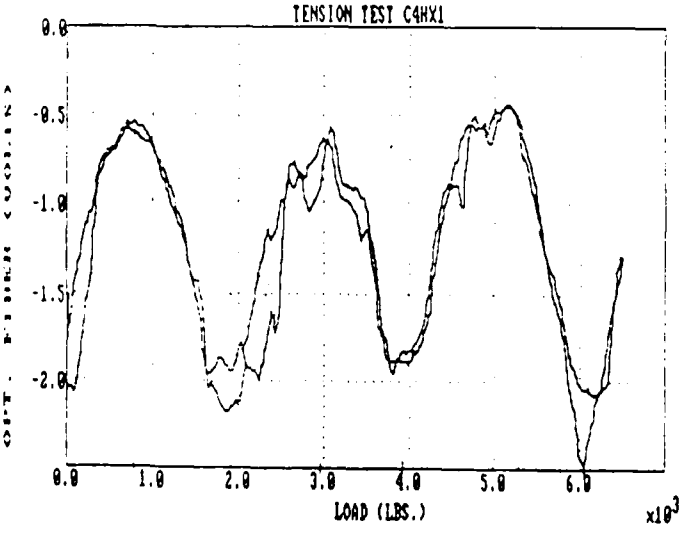

FIGURE 8. POLARIMETRIC INSTRUMENTATION VERIFICATION DATA

The coupon was loaded as shown in Figure 6. Measurements one through six were taken for both the high and low birefringence fiber. Representative data is shown in Figure 8. Optical responsivity for each case was determined by performing a linear polynomial least squares fit of the fringe count (each successive peak or valley represents one half a fringe) to the strain applied. The slope of the line divided by the embedded (gage) length (1") gives the optical responsivity. Table 4 shows data reduction for measurement configuration #1 (Figure 8) for the low and high birefringence fiber while Table 5 lists optical responsivity calculated for each measurement.

Several points can be made about the data

1. Low birefringence fiber exhibited little or no hysteresis.
2. High birefringence fiber was sensitive to transverse strain (86% relative to low birefringence).
3. Considerable "noise" is present in the high birefringence fiber data.

Noise was attributed to laser diode wavelength stability and its interaction with 5 meters of high birefringence optical lead. Total retardation through the five meters, assuming a 2mm beat length is:

$$\text{Total retardation} = \frac{820\ \text{nm}}{2\frac{\text{mm}}{\text{fringe}}} \cdot 5\text{m} \cdot \frac{1000\ \text{mm}}{\text{m}} = 2.05 \times 10^{6}\ \text{nm}$$

$$= 2500\ \text{fringes @ } 820\ \text{nm}$$

A one fringe change, given the same total retardation, can be caused by a wavelength shift to

$$\lambda = \frac{\text{Total retardation}}{\#\ \text{of fringe}} = \frac{2.05 \times 10^{6}\ \text{nm}}{2499\ \text{fringes}} = 820.33\ \text{nm}$$

In other words a .33 nm change in laser diode wavelength can cause a one fringe change in signal output. The wavelength-temperature coefficient of the Hitachi HLP-1400 used was .2 - .3 nm/°C. A one degree C change in laser diode temperature is therefore capable of a one fringe change in signal output. Data presented in Figure 8 shows about 10% of a fringe. Since the laser diode environment was not controlled, wavelength temperature variation could easily account for the above noise.

TABLE 4. POLARIMETRIC DATA REDUCTION

LOW BIREFRINGENCE FIBER

Retardation (fringes)	Load (Lbs.)	Strain (%)
0.5	459	.014
1.0	1359	.042
1.5	2294	.072
2.0	3247	.101
2.5	4147	.129
3.0	5082	.159
3.5	6000	.187

LEAST SQUARES FIT

Fringes = 17.28 fringe/% ε_t • % ε_t + .262 fringe

Optical responsivity = 17.28 fringe/% ε_t • in

HIGH BIREFRINGENCE FIBER

Retardation (Fringes)	Load (Lbs.)	Strain (%)
0.5	776.	.024
1.0	1906.	.059
1.5	2965.	.092
2.0	3935.	.122
2.5	4994.	.155
3.0	6053.	.187

LEAST SQUARES FIT

Fringes = 15.43 fringe/% ε_t • % ε_t + .106 fringe

Optical responsivity = 15.43 fringe/% ε_t • in

TABLE 5. INSTRUMENTATION VERIFICATION OPTICAL RESPONSIVITY

MEASUREMENT #	LOW BI RESPONSIVITY (Fringe/% ε • in)	HIGH BI RESPONSIVITY (Fringe/% ε • in)
#1	17.28	15.43
#2	17.28	14.85
#3	17.27	14.80
#4	17.25	14.55
#5	17.07	14.79
#6	17.47	14.71
AVE.	17.28	14.85
STD. DEV.	.12 (.75%)	.30 (2%)

Low birefringence fiber data does not exhibit observable noise because the total optical retardation is small. Three fringes are visible in the data during coupon loading and another 1 fringe can be assumed due to residual static birefringence in the optical fiber leads to and from the coupon. Total retardation is written as:

$$\text{Total retardation} = 4 \text{ fringes} \cdot 820 \text{ nm /fringe}$$
$$= 3280 \text{ nm}$$

A change of .33 nm in laser wavelength appears as:

$$\#\text{ fringes @ } 820.33 = \frac{3280 \text{ nm}}{820.33 \frac{\text{nm}}{\text{fringe}}} = 3.998 \text{ fringes}$$

or a .002 fringe change.

In comparison, a .33 nm wavelength change with high birefringence fiber causes a 1 fringe change in signal output under similar conditions. It should be noted that if 5 meters of low birefringence optical fiber is loaded to the level of stress which exists in high birefringence fiber, the output will exhibit the same level of wavelength sensitivity.

Single mode laser diodes also change wavelength, or mode hop, due to fluctuations in drive current. Wavelength change with drive current is typically .2 nm/10 milliamp. Feedback loop stability of $\pm$10 microwatts is equivalent to current stability of $\pm$.0022 mA. Wavelength excursion is calculated as:

$$\text{Wavelength change} = \frac{.2 \text{ nm}}{10 \text{ mA}} (\pm .0022 \text{ mA})$$
$$= \pm 4.4 \times 10^{-5} \text{ nanometers}$$

Wavelength changes due to drive current changes are insignificant compared to temperature driven changes.

Optical leads to and from the coupon totaled about five meters which would probably be on the short side for an aircraft application. Stringent thermal stability requirements would be placed on the electronic cooling system in practice. (Gas lasers have better wavelength/temperature characteristics but are considerably larger than laser diodes.)

2.3 Coupon Four Point Bend Test

Four point bend testing was performed on coupon types "A", "B", "C" and "E". Inner load rollers were 4.5" apart and centered while outer load rollers were 9.0" apart and centered. Data was taken and reduced as described in the previous section. Coupon optical responsivity is listed in Table 6. Analysis of the above data is performed in section 2.6.

It should be noted that coupon optical responsivity is referenced to measured strain which is not necessarily the strain seen by the optical fiber.

2.4 Coupon Compression Testing

Compression testing was performed on the "D" coupons and control coupons "F". The phase of the optical signal was not related to coupon strain in a linear manner. Nonlinearities are attributed to creep in the adhesive between the coupon and aluminum end tabs.

Figure 9 shows axial strain gage, stroke and optical signals versus load. Strain is linear with load as might be expected. Stroke, however, has a clear slope change at 800 lbs. during loading and 600 lbs. during unloading. Mechanical compliance must exist in the coupon/end table/load frame system which is not present at the strain gage location. The optical signal also responds to the load in a nonlinear fashion. Fringe rate (w.r.t. load) is low before the slope change and high after.

Since the optical signal is responding with stroke and the strain gage is not, the additional excitation must be located where the embedded optical fiber runs between the hydraulic grips. Therefore the source of the mechanical compliance, is probably creep in the adhesive which bonds the aluminum end tabs to the coupon.

The hydraulically controlled grips may be providing an additional load in reaction to adhesive creep. Pressure in the grip is controlled to constant pressure during loading. Adhesive creep may

upset the equilibrium condition and change the load across the coupon and hence across the embedded fibers. Figure 10 shows the optical signal when the grip is pressurized but the coupon is not loaded in the 0° direction. Clearly, the optical fibers are capable of sensing loading by the grips.

Uniaxial 0° tension, not compression, was applied during the data collected in Figure 9. It was recognized that bending and/or buckling could occur during 0° compression and further complicate the load on the fiber. To minimize the possible load conditions, test were performed in 0° tension.

2.5 Coupon Loading to Failure

The coupons used for the four point flex and compression tests were loaded to failure. Coupon types "A", "B", "C", and "E" were loaded in 0° uniaxial tension while "D" and "F" coupons were loaded in 0° uniaxial compression. The objective of the test series was to determine if embedded optical fibers have any adverse effect on coupon strength.

Three groups of coupon types were failed in tension - two with embedded optical fibers and one without to act as a control. Three replicates of each coupon type were tested to failure. Coupon end tabs were aluminum. Dimensions were 1.5" wide, 2.5" long by 1/16" thick. Hysol 934 NA epoxy was used to attach the end tabs to the aluminum. The results of the tension test are listed in Table 7.

Two groups of coupon types were failed in compression - one with embedded optical fibers and one without to act as a control As with the tension coupons, three replicates for each group were tested to failure. The results of this series of tests are listed in Table 8.

A stress concentration caused all the test coupons for both tensile and compressive tests to fail at the end tabs rather than in the gages section. The cause of this failure is not known but is suspected to be related to fabrication of the test articles.

Taking into account the facts that none of the test samples failed in the gage section and that a small number of test replicates were used, the data from these tests does not indicate any trend of composite strength reduction. A more accurate appraisal of strength reduction could be obtained by performing further tests with larger sample populations.

TABLE 6. FOUR POINT BEND TEST OPTICAL RESPONSIVITY

COUPON TYPE	COUPON NUMBER	LOW BIREFRINGENCE #1 FRINGE/%ε • in	HIGH BIREFRINGENCE FRINGE/%ε • in	LOW BIREFRINGENCE #2 FRINGE/%ε • in
A	1	F	.44	F
	2	F	F	F
	3	F	F	F
B	1	F	F	F
	2	.49	F	F
	3	F	F	F
	4	-	NT/.85/1.03	-
C	1	F	NT	4.77
	2	F	5.33	F
	3	F	5.47	6.55

F = Failed Optical Continuity Test
NT = Not tested, Fiber broken external to coupon, too short for splicing

FIGURE 9. COUPON TENSILE TEST DATA PLOT

RESISTIVE STRAIN GAGE

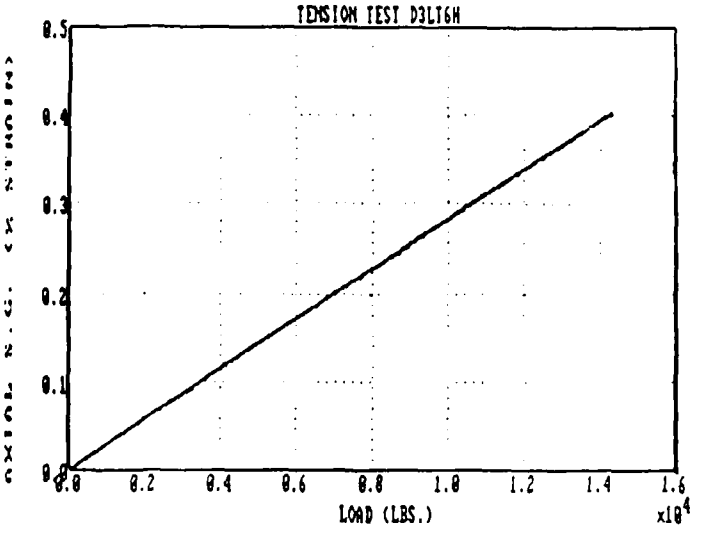

STROKE

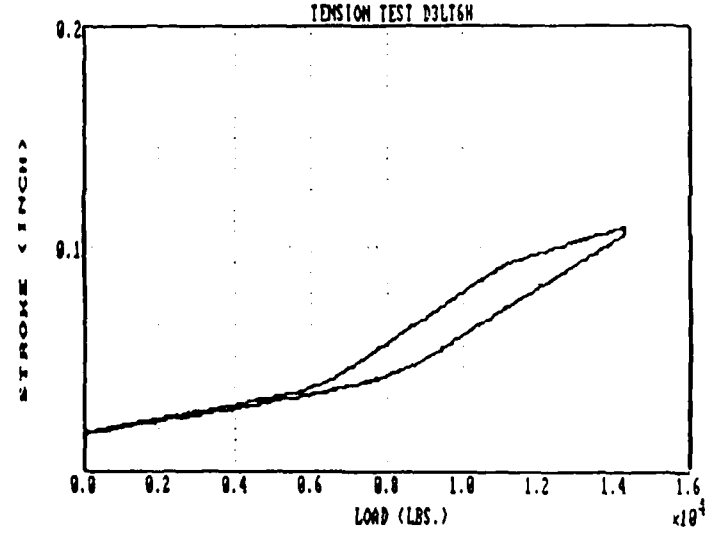

OPTICAL SIGNAL

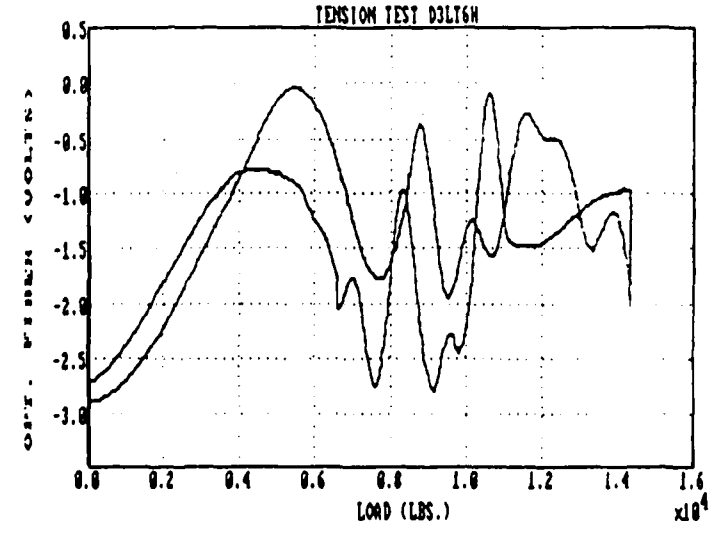

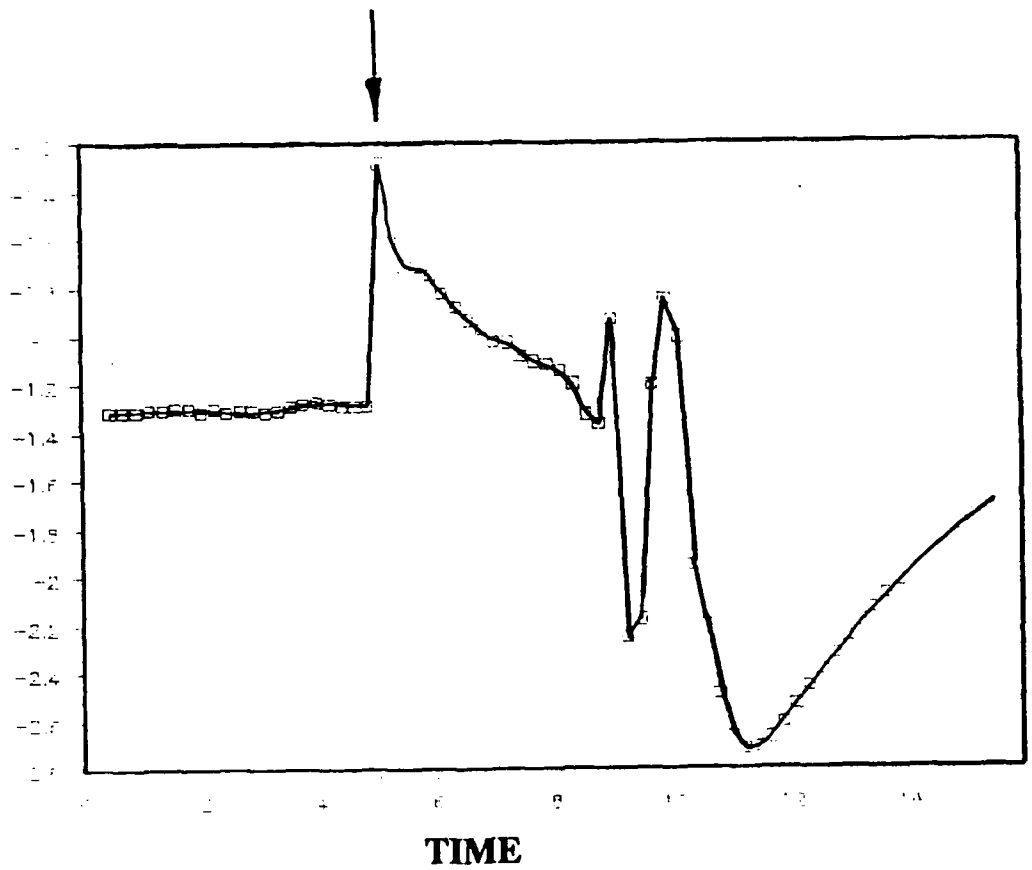

FIGURE 10. GRIP PRESSURIZATION DATA PLOT

2.6 Coupon Test Analysis

This section presents previously developed theory and provides comparison to empirical data. Since strain was measured on the surface and the fiber was embedded, it was sometimes necessary to develop a relationship between strain at the resistive strain gage location and strain at the optical fiber location.

Theoretical

Theory is available for the situation presented by the "C" configuration coupon when loaded in pure tension (Section 2.2) or four point bending. The optical fibers are perpendicular to the graphite fibers and away from the center line. In both cases a circular elastic inclusion in an orthotropic plate forms a reasonable model for the situation. Figure 11 depicts the model.

Theory is also available for the situation presented by the "B" configuration in four point bending. In this case the optical fibers and graphite fibers are aligned. Since the optical fiber is off center, an axial load is applied. The situation is depicted in Figure 11.

Transverse Responsivity

The photoelastic effect[4] in two dimensions is given as:

$$\begin{bmatrix} \tilde{n}_1 \\ \tilde{n}_2 \end{bmatrix} = \begin{bmatrix} n_1 \\ n_2 \end{bmatrix} + \begin{bmatrix} Q_{11} & Q_{12} \\ Q_{12} & Q_{11} \end{bmatrix} \begin{bmatrix} \sigma_1 \\ \sigma_2 \end{bmatrix} \tag{2.6-1}$$

where: n_1, n_2 - principal indices of refraction of unstressed material
$\tilde{n}_1, \tilde{n}_2$ - principal indices of refraction of stressed material
σ_1, σ_2 - principal stresses
Q_{11}, Q_{12} - direct and transverse opto-elastic constants of stress material

TABLE 7. COUPON FAILURE TEST RESULTS - TENSION

COUPON TYPE	SPECIMEN NUMBER	FAILURE STRESS (KSI)	FAILURE STRAIN (%)	MODULUS (MSI)
A	1	157	1.02	15.4
	2	162	1.00	16.2
	3	183	1.11	16.5
	Average	167	1.04	16.0
	Std. Dev.	11.3 (7%)	0.05 (5%)	0.5 (2%)
C	1	124	0.79	15.7
	2	118	0.79	14.9
	3	114	N/A	N/A
	Average	119	0.79	15.3
	Std. Dev.	4.1 (3%)	0.0	0.4 (3%)
E	1	170	1.03	16.5
	2	93	0.61	15.2
	3	167	1.05	15.9
	Average	143	0.90	15.9
	Std. Dev.	44 (31%)	0.24 (27%)	0.6 (4%)

Note: B coupon not tested. Failed during OTDR testing.

TABLE 8. COUPON FAILURE TEST RESULTS - COMPRESSION

COUPON TYPE	SPECIMEN NUMBER	FAILURE STRESS (KSI)	FAILURE STRAIN (%)	MODULUS (MSI)
D	1	125	0.79	15.8
	2	146	0.93	15.7
	3	98	0.65	15.1
	Average	123	0.79	15.5
	Std. Dev.	24 (20%)	0.14 (2%)	0.4 (2%)
F	1	97	0.58	16.7
	2	134	0.77	17.4
	3	139	0.83	16.7
	Average	123	0.73	16.9
	Std. Dev.	23 (19%)	0.13 (78%)	0.4 (2%)

Transit times, t, through an optical material of length L in the 1 and 2 directions are

$$t_1 = \frac{L}{V_1} = L\frac{\tilde{n}_1}{C} \tag{2.6-2}$$

and

$$t_2 = \frac{L}{V_2} = L\frac{\tilde{n}_2}{C} \tag{2.6-3}$$

where: V_1, V_2 - speed of light in optical material
C - speed of light in a vacuum

The phase difference in fringes is simply the transit time difference relative to the optical period, T, and written as:

$$\Delta\phi = \frac{t_1 - t_2}{T} \tag{2.6-4}$$

Equations (2.6-2), 2.6-3) and (2.6-4) are combined to yield

$$\Delta\phi = \frac{L}{CT}\left(\tilde{n}_1 - \tilde{n}_2\right) \tag{2.6-5}$$

which is rewritten

$$\Delta\phi = \frac{L}{\lambda}\left(\tilde{n}_1 - \tilde{n}_2\right) \tag{2.6-6}$$

where λ is the free space optical wavelength. Substitution of Equation (2.6-1) into (2.6-6) gives:

$$\Delta\phi = \frac{L}{\lambda}(Q_{11} - Q_{12})\,(\sigma_1 - \sigma_2) \tag{2.6-7}$$

The opto-elastic constants are combined as:

$$Q = Q_{11} - Q_{12} \tag{2.6-8}$$

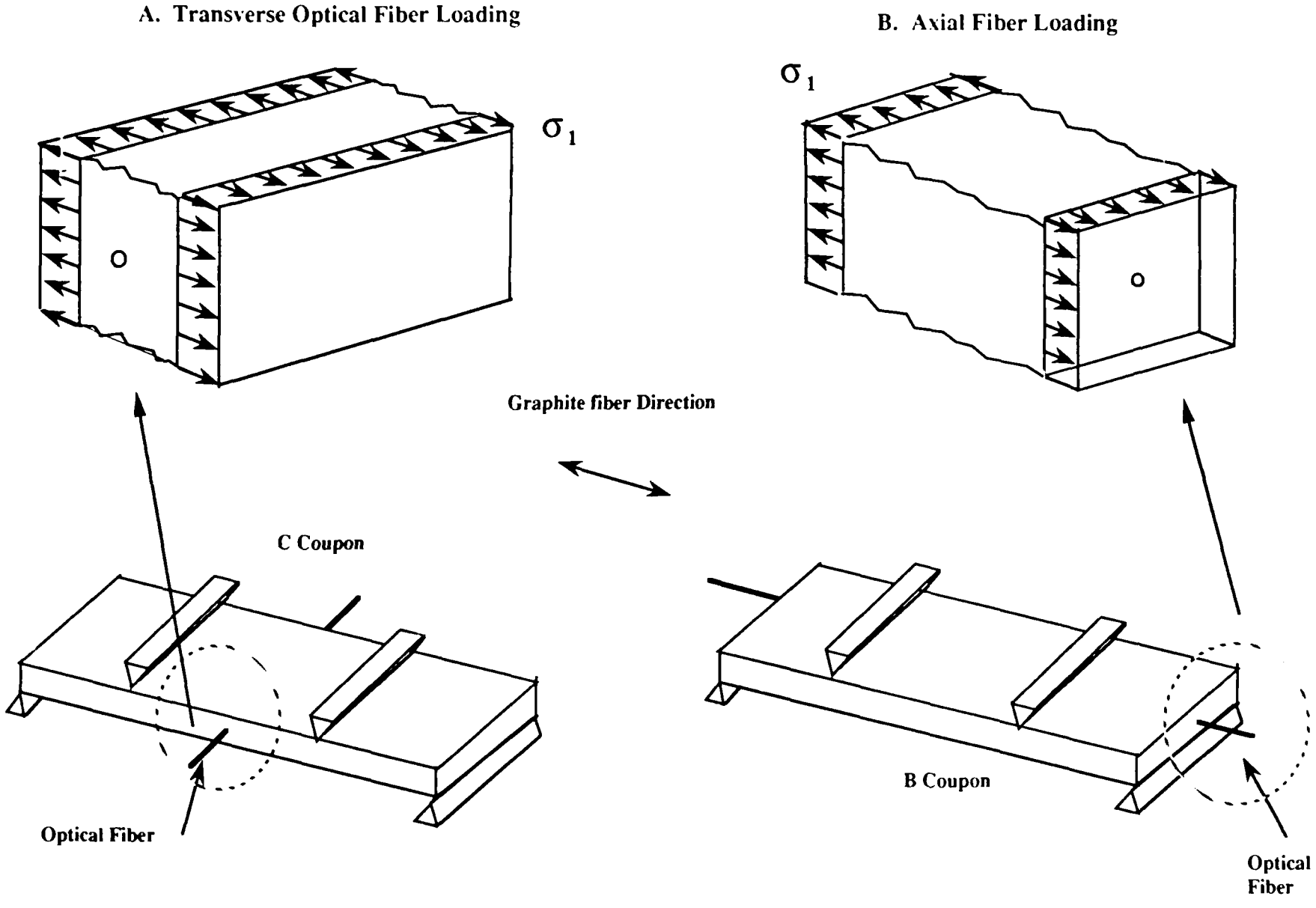

FIGURE 11. OPTICAL FIBER LOADING MODELS

which has a value[4] of 3.27 X 10^{-5} mm^2/kg (2.2983 x 10^{-8}/psi). Phase change can now be written as:

$$\Delta\phi = \frac{L}{\lambda} Q(\sigma_1 - \sigma_2) \tag{2.6-9}$$

Transverse loading conditions produce strain perpendicular to the core of the optic fiber. Equation (2.6-9) is manipulated to give optical responsivity (phase change per length per strain).

The principal stress difference[2] is given by :

$$\sigma_1 - \sigma_2 = 2\bar{\sigma}_1 D_2 \tag{2.6-10}$$

where: σ_1 = average coupon stress
D_2 = .436

Parameter, D_2, defines the coupling between the coupon and the optical fiber as a function of elastic constants.

Average stress is converted to average strain using Hooke's Law:

$$\bar{\sigma}_1 = E_{11}\bar{\varepsilon}_t \tag{2.6-11}$$

where: E_{11} = Young's Modulus in stress direction (18.5 x 10^6 psi for G/E composite)
ε_1 = Average coupon strain in stress direction

Fiber transverse responsivity, n_t, is calculated as:

$$n_t = \frac{\Delta\phi}{\bar{\varepsilon}_1 L} = 2D_2\frac{Q}{\lambda} E_{11} \tag{2.6-12}$$

$$= 2(.436)\frac{2.2983 \times 10^{-8}/\text{psi}}{820 \times 10^{-6}\,\frac{\text{nm}}{\text{cycle}} \cdot \frac{1\text{ in}}{25.4\text{ mm}}} \cdot 18.5 \times 10^{6}\text{ psi} \cdot \frac{1\text{ fringe}}{\text{cycle}} \cdot \frac{1\text{ strain}}{100\,\%\text{ strain}}$$

$$= 114.8\ \frac{\text{fringe}}{\%\,\varepsilon_t \cdot \text{ in}}$$

No theoretical results are available for transverse strain response of a high birefringence fiber. However, the following assumptions were made:

- Since the core material of a low birefringence is the same as a high birefringence fiber, the same average (in a directional sense) transverse responsivity should be obtained (i.e 114.8 fringe/ $\%\varepsilon \cdot$ in)

- Since an asymmetry exists in the cladding material of a high birefringence fiber, responsivity should be a function of the direction of the applied load with respect to the principal axes of the optical fiber.

Axial Responsivity

Two effects cause high birefringence fiber to have axial strain sensitivity. One is due to a physical lengthening of the optical path as mentioned previously. The second is due to the transverse Poisson contraction during axial strain. Asymmetries cause different contractions in the X and Y directions and hence a differential transverse strain. Birefringence is increased due to axial strain.

The describing equation [6] for stress induced birefringence is:

$$n_z = \frac{1}{L_B}\ \frac{V_2 - V_1}{(\alpha_2 - \alpha_1)\,T} \qquad (2.6\text{-}13)$$

where: V_1, V_2 = Poisson Ratio of fiber cladding and stress lobe

α_1, α_2 = Thermal expansion of fiber cladding and stress lobe

$$\frac{V_2 - V_1}{(\alpha_2 - \alpha_1)T} = 20$$

For the 2mm beat length fibers used the axial responsivity is:

$$n_z = \frac{25.4 \text{ mm}}{\frac{2 \text{ mm}}{\text{fringe}} \cdot \text{in}} \; 20 \cdot \frac{1 \text{ strain}}{100\% \text{ strain}}$$

$$= 2.54 \frac{\text{fringe}}{\% \, \varepsilon_z \cdot \text{in}}$$

The responsivity given above should be considered an upper limit. Reference 6 assumed a free boundary at the cladding. Embedment as shown in Figure 11 would not allow a differential radial contraction as the wall is restrained by the composite. A lower limit can be placed on axial strain responsivity by assuming the optical signal is due only to the path length change. For example, if a length, L, of optical fiber with a 2 mm beat length is stretched 2 mm, a one fringe change is optical signal will occur. Response can be determined as:

$$n_z = \frac{1 \text{ fringe}}{\frac{2 \text{ mm}}{L} \cdot L} \cdot \frac{1 \text{ strain}}{100\% \text{ strain}} \cdot \frac{25.4 \text{ mm}}{\text{in}}$$

$$= .127 \frac{\text{fringe}}{\% \, \varepsilon_z \cdot \text{in}}$$

Comparison of transverse and axial strain responsivities shows that analytically, transverse strain is at least 45 times higher than axial strain.

Empirical

Transverse Response

Transverse strain responsivity was determined experimentally in two situations: Instrumentation Verification Testing (section 2.2) and Coupon "C" Four Point Flex Testing. Instrumentation Verification Testing data is presented as is. The strain measured at the surface is representative of the average strain in the coupon. This is not true for the four point flex test. Strain at the optical fiber layer is one half the strain measured at the surface. Optical responsivities are doubled before presentation in Table 9 for the four point bend test.

Two conclusions can be drawn from this data. One is that experimental data is only 15% of predicted. A resin pocket forms around the optical fiber when the graphite fiber and optical fiber are perpendicular to each other. The model, which assumes macroscopic elastic constants does not maintain complete fidelity at the microscopic level. Comparison of high and low birefringence fiber responsivities shows that high birefringence fiber is 5 to 14% as responsive as low birefringence optical fiber. It appears that the stress lobes built into the fiber have a small but not insignificant effect on transverse responsivity.

Axial Response

Determination of the axial response of the high birefringence fiber required some manipulation. The load points in the four point bend tests applied a load normal to the fibers. High birefringence fibers, which were embedded off axis for elongation, receive both normal and axial loading.

Isolation of the axial loading occurred by comparison of "A" and "B" coupon results. Optical fibers were loaded by the supports in both cases but differed in tensile loading. "A" coupons had the optical fibers on the neutral axis while "B" coupons were embedded off axis. "A" coupon responsivity was subtracted from "B" coupon responsivity to remove the effects of point loading.

TABLE 9. THEORETICAL AND EXPERIMENTAL COMPARISON OF TRANSVERSE STRAIN RESPONSIVITY

TEST DESCRIPTION	LOW BIREFRINGENCE fringe/ % ε • in	HIGH BIREFRINGENCE FIBER (fringe/ % ε • in)	RATIO
Instrumentation Verification			
• Theoretical	114.8	114.8	1
• Experimental	17.3	14.9	.86
Four Point Bend Test C Coupons			
• Theoretical	114.8	114.8	1
• Experimental	17.0	16.2	.95

$$n_z = .94 \frac{\text{fringe}}{\%\,\varepsilon \cdot \text{in}} - .44 \frac{\text{fringe}}{\%\,\varepsilon \cdot \text{in}}$$

$$= .5 \frac{\text{fringe}}{\%\ \varepsilon \cdot \text{in}}$$

The reference strain gage measures strain at the center of the beam span while the optical fiber integrates strain along the embedded length. Figure 12 depicts the situation. Strain at the center and integrated strain (both at the surface) are related by:

$$\Delta L\ (h) = \int_0^L \varepsilon_{zm}(h)dz = \frac{3}{4}\varepsilon_{zm} L \tag{2.6-14}$$

where h is the half thickness of the beam and ε_{zm} is the measured surface strain at the beam center. The elongation at the optical fiber is reduced by a factor of two as compared to surface elongation:

$$\Delta L(h/2) = \frac{1}{2}\Delta L(h) = \frac{3}{8}\varepsilon_t L \tag{2.6-15}$$

or

$$\frac{\Delta L}{L}\ (h/2) = \frac{3}{8}\varepsilon_{zm} = \varepsilon_{z0} \tag{2.6-16}$$

where ε_{z0} is the average strain along the optical fiber. Axial responsivity of the optical fiber can be determined by scaling the coupon response as:

$$n_z = \frac{.5\ \text{fringe}}{\%\ \varepsilon_{zm} \cdot \text{in}} \cdot \frac{8}{3} \frac{\%\varepsilon_{zm}}{\%\varepsilon_{z0}} = 1.33 \frac{\text{fringe}}{\%\ \varepsilon_{z0} \cdot \text{in}}$$

Axial responsivity is within the range (.13 - 2.5 fringe/% ε • in) predicted by theory.

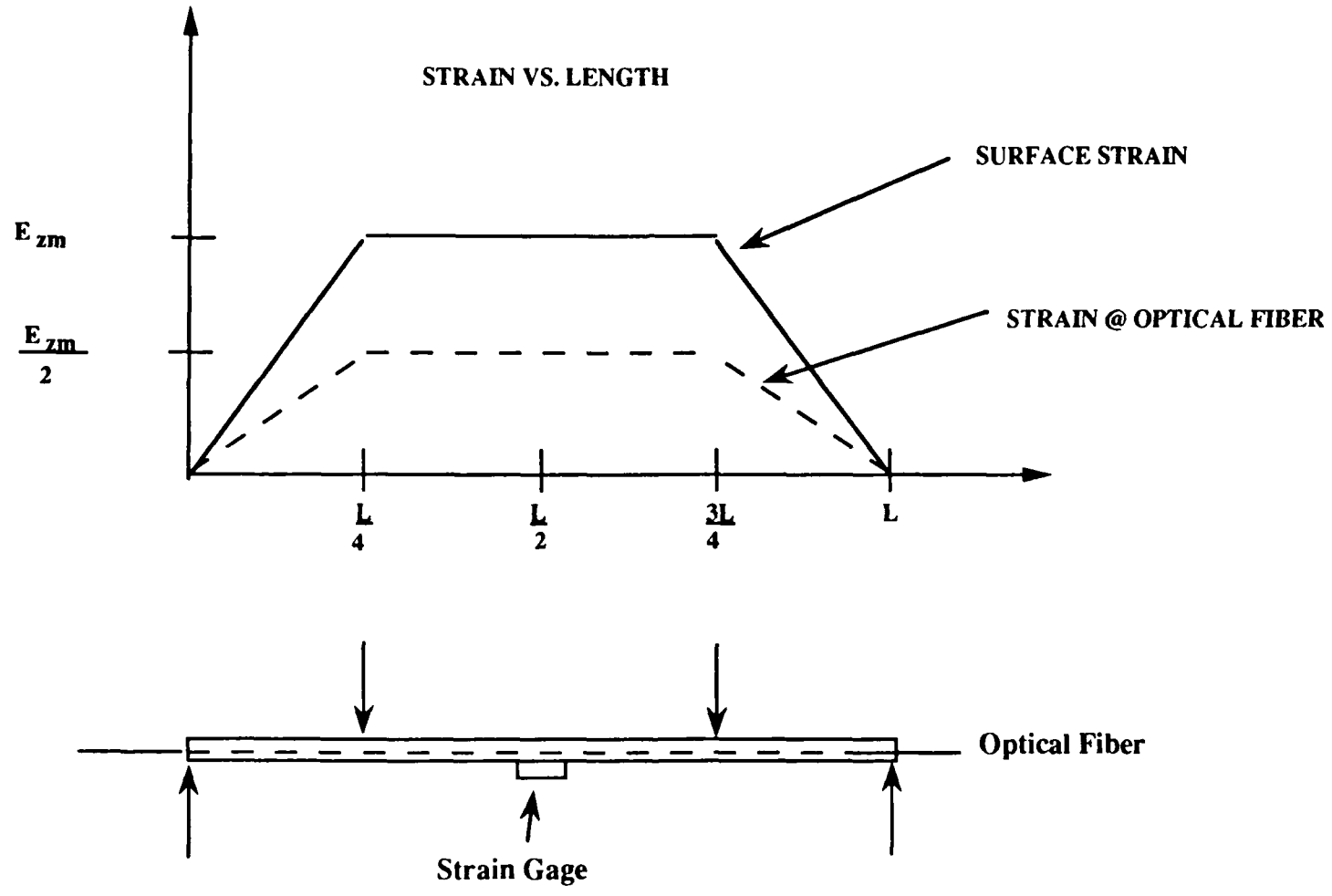

FIGURE 12 . FOUR POINT BEND STRAIN DISTRIBUTION

Transverse strain responsivity of high birefringence optical fibers is larger than axial responsivity in both an empirical and theoretical sense. Therefore, high birefringence fiber is not recommended for use as an axial strain gage.

2.7 OTDR Testing

OTDR testing was originally scheduled to be performed in four point bending as shown in Figure 13. An Anritsu MW920A OTDR with 830 nm optics was used in testing. Optical pulse width was 3 nanoseconds. One hundred pulse cycles were averaged to form a trace.

Initial OTDR testing showed no response when loaded to 6000 lbs. in four point bending. Point load separation of 2.5 inches defines system resolution requirements. Instrument resolution was tested by placing a 1/4" diameter bend in an optical lead as shown in Figure 13. OTDR traces with and without the bend are shown in Figure 14 in the lower and upper traces, respectively. Comparison of the traces clearly identifies the location of the bend in the lead. Instrument cursors are used to measure the distance for the system to respond to the input. Response from beginning to end of the optical power loss is 1.2 meters. This measurement is the spatial analog to a four time constant step response in an electrical circuit. OTDR resolution is inadequate for the application under discussion.

OTDR response limitations are driven by optical pulse width. A 3 ns pulse occupies about 2 feet in the optical fiber. Point loads within one pulse, or 2 feet therefore, spatially cannot be accurately resolved. Shorter pulses with higher power are required for better resolution.

Resolution limitations were overcome by cascading three coupons in series. Figure 15 depicts the experimental configuration. Approximately four meters separated the load points. Load area was .28 square inches. Compressive loads ranged from 0 to 18,000 lbs. for a stress range of 0 - 64,000 psi. Experimental traces are shown in Figure 16.

Load points do not become visible until 64,000 psi. This is in the vicinity of the failure strength of the material. This indicates a suitable application of OTDR technology may be damage detection. Sensitivity to load may be improved by replacing the optical fiber acrylate buffer with a material which transfers stress to the optical fiber better.

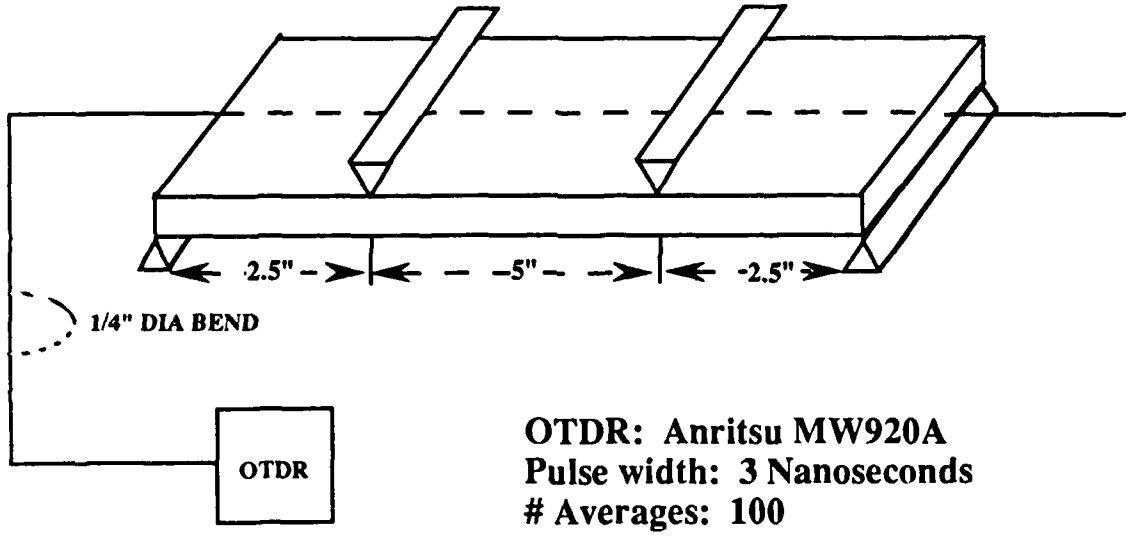

FIGURE 13. INITIAL OTDR TESTING SCHEMATIC

Reference Trace

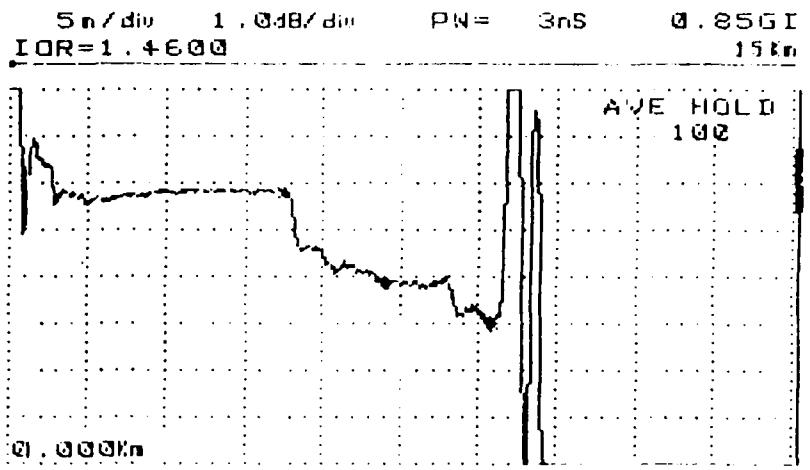

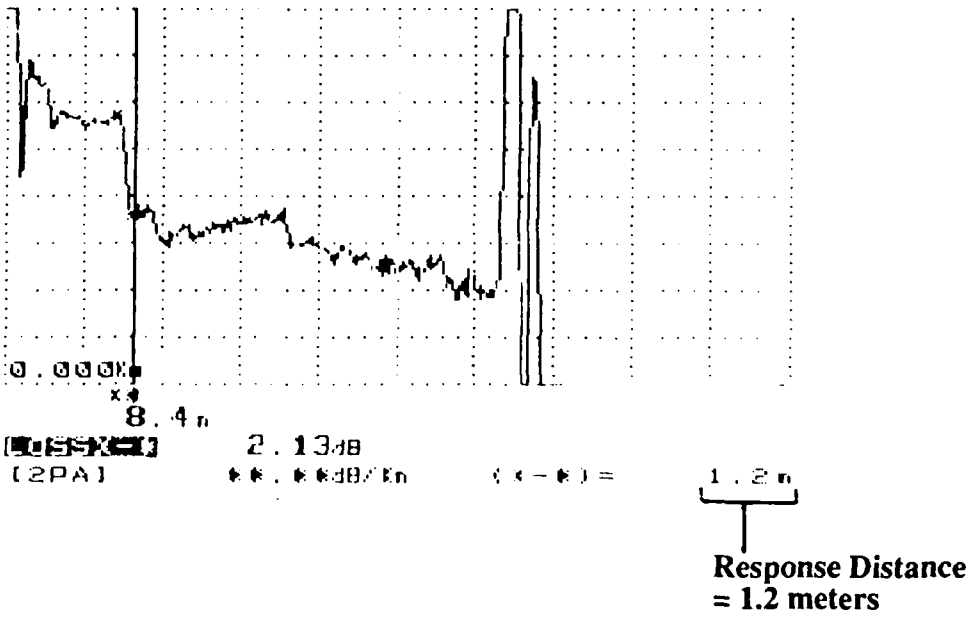

1/4" Dia. Optical Fiber Bend @ 8 meters

FIGURE 14. OTDR RESOLUTION TEST TRACES

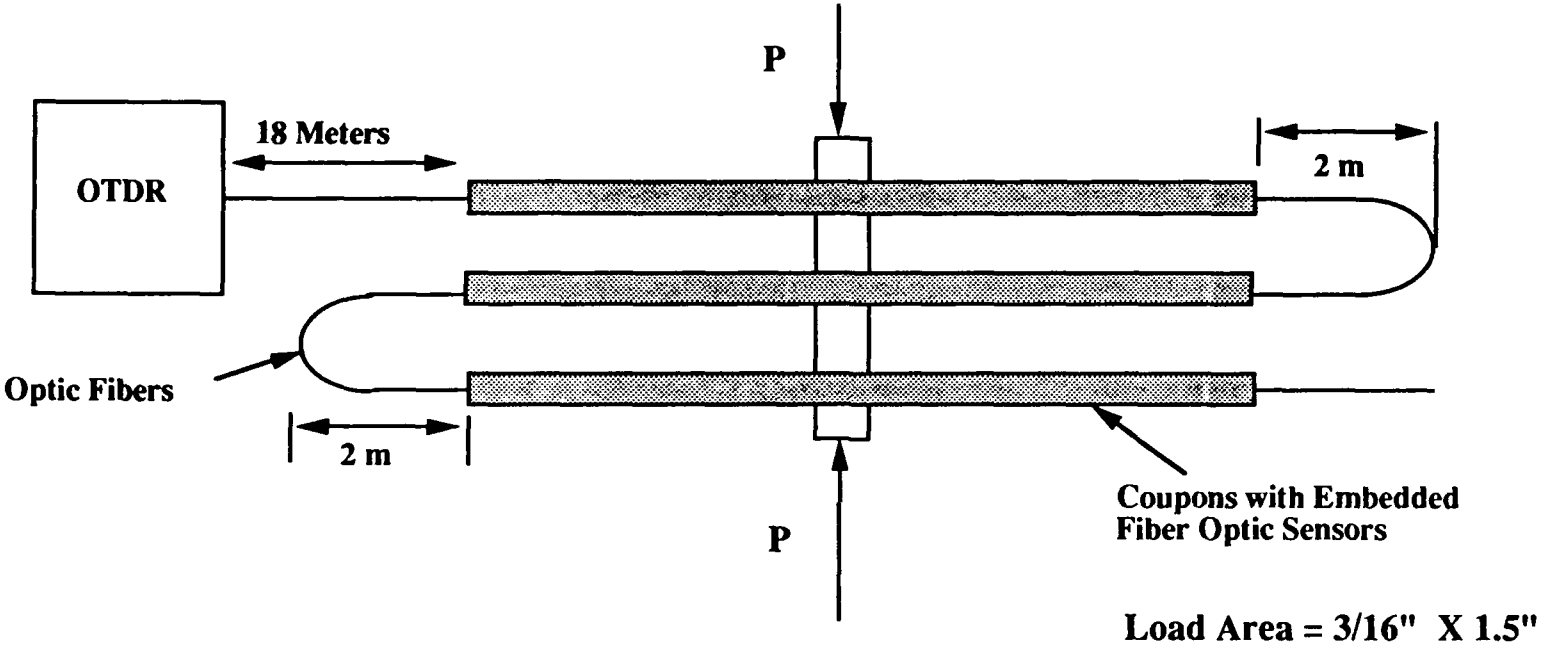

FIGURE 15. REVISED OTDR TEST SCHEMATIC

0 PSI

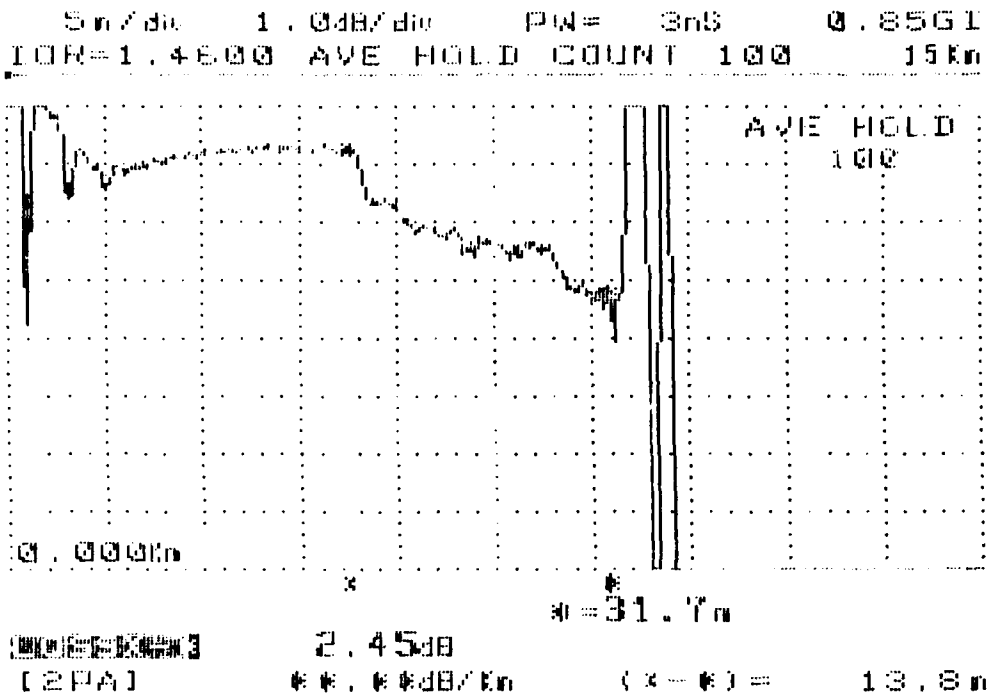

18,000 PSI

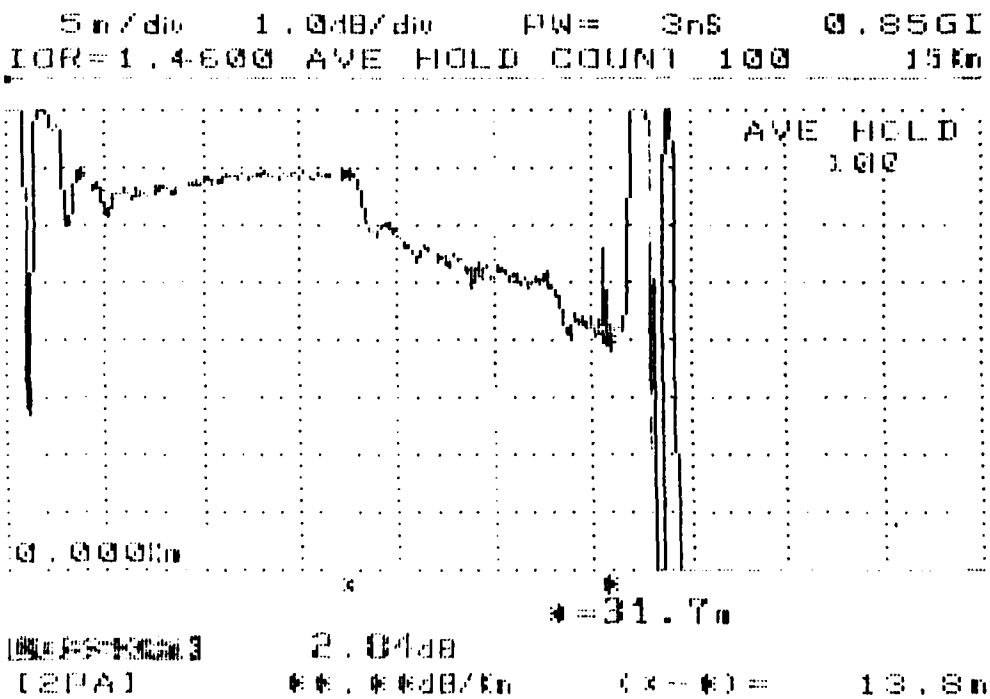

FIGURE 16. REVISED OTDR TEST TRACES

32,000 PSI

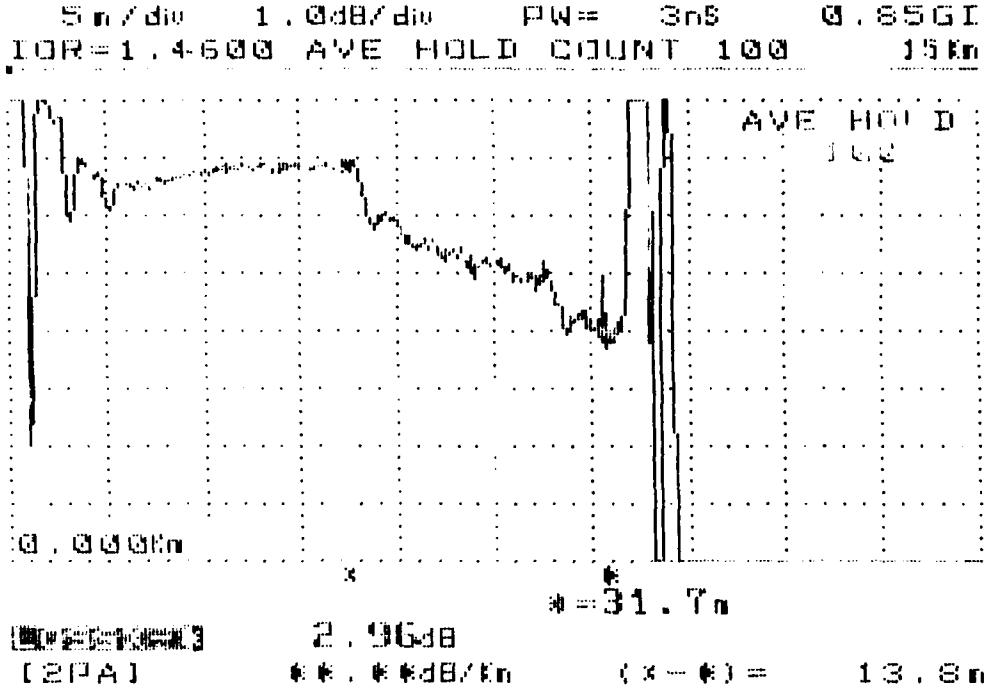

50,000 PSI

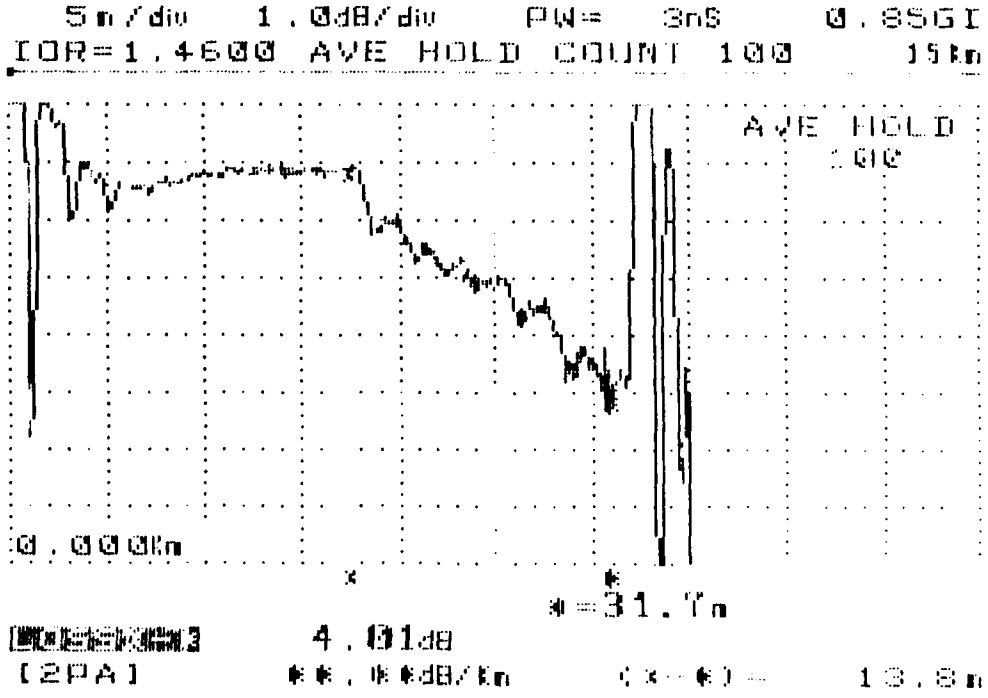

FIGURE 16. REVISED OTDR TEST TRACES (CONT.)

64,000 PSI

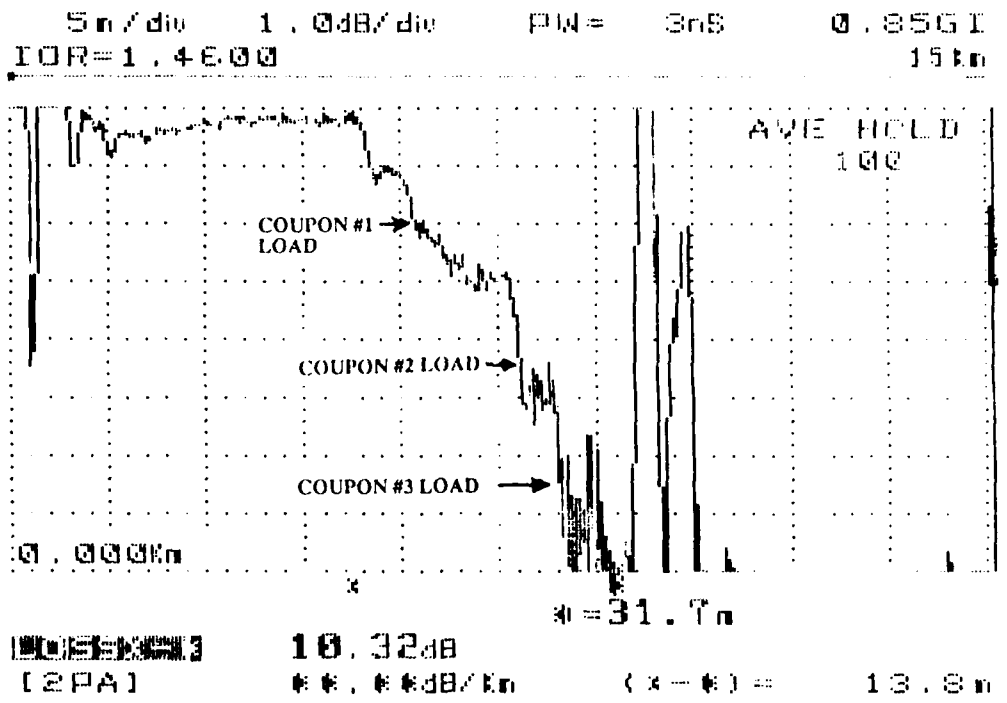

0 PSI

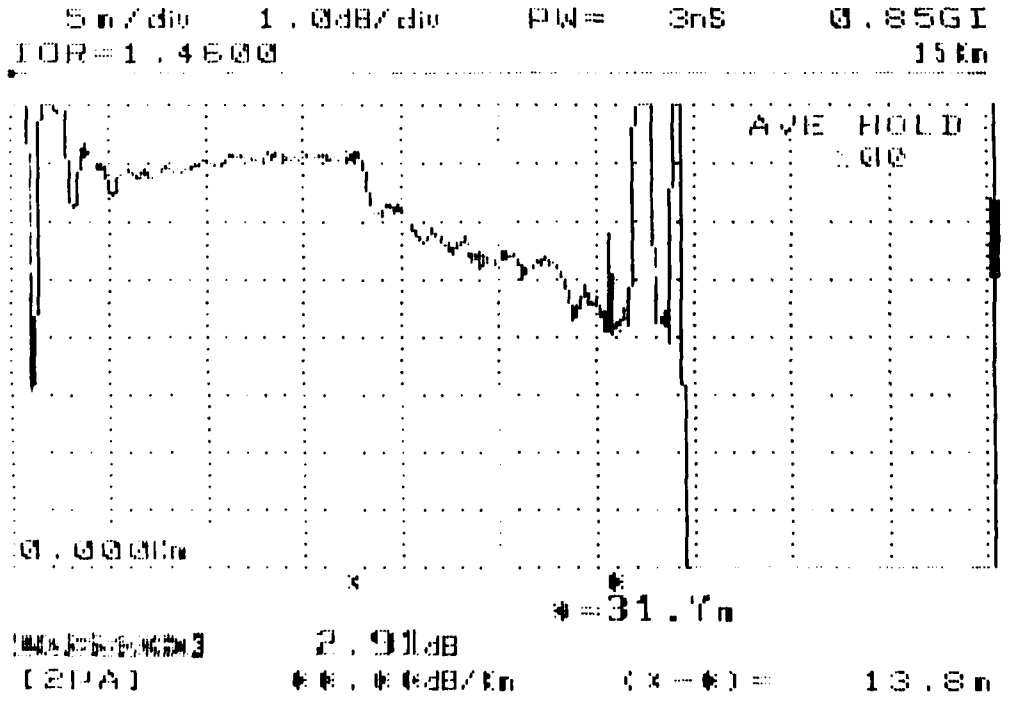

FIGURE 16. REVISED OTDR TEST TRACES (CONT.)

3.0 I-BEAM STRUCTURAL FABRICATION AND TESTING

Preliminary Fabrication and Testing (section 2.0) consisted of embedding 3 types of fiber optic sensors in a simple composite structure (i.e. coupons) at various orientations with respect to the load and the graphite fibers within the coupon. Knowledge gained from this testing was used for the design of a more complicated structure with embedded fiber optic sensors. This section describes the fabrication and testing of a composite I-beam with embedded fiber optic sensors.

3.1 I-Beam Design

I-Beam geometry is shown in Figure 17 while Figure 18 depicts the I-beam layup. Low birefringence polarimetric sensors were embedded in the I-beam. These sensors were shown to be effective in measuring strain applied normal to the optic fiber axis. High birefringence polarimetric sensors and multimode OTDR sensors were not embedded because axial strain measurement (with respect to the optical fiber) using the polarimetric technique combined with high birefringence fiber was ineffective due to sensitivity to transverse strain and laser diode wavelength sensitivity. OTDR sensors were not employed due to the resolution limitation mentioned previously.

Low birefringence fibers were mounted in the flanges, perpendicular to the beam length, between the load points. Orientation of the optical fibers perpendicular to the length aligns the sensitive axis of the optical fiber with the strain field. Optical fibers were located two plies from the surface of the beam. The largest optical response occurs away from the beams neutral axes. Furthermore, the same local environment, as compared to coupon fabrication, was maintained, i.e. optic fibers were mounted perpendicular to graphite fibers. Resistive strain gages were mounted halfway between optical fibers, top and bottom.

Gold buffered low birefringence (632 nm) fibers were embedded in the I-beam. The 15 micron thick gold buffer was rated to 750°C and was expected to improve survivability both during cure and subsequent handling.

3.2 I-Beam Fabrication

Two I-beams were fabricated as shown in Figure 29. Four gold coated fibers were embedded in an attempt to improve the optical fiber survival rate. Table 10 indicates survival rate and gold fiber

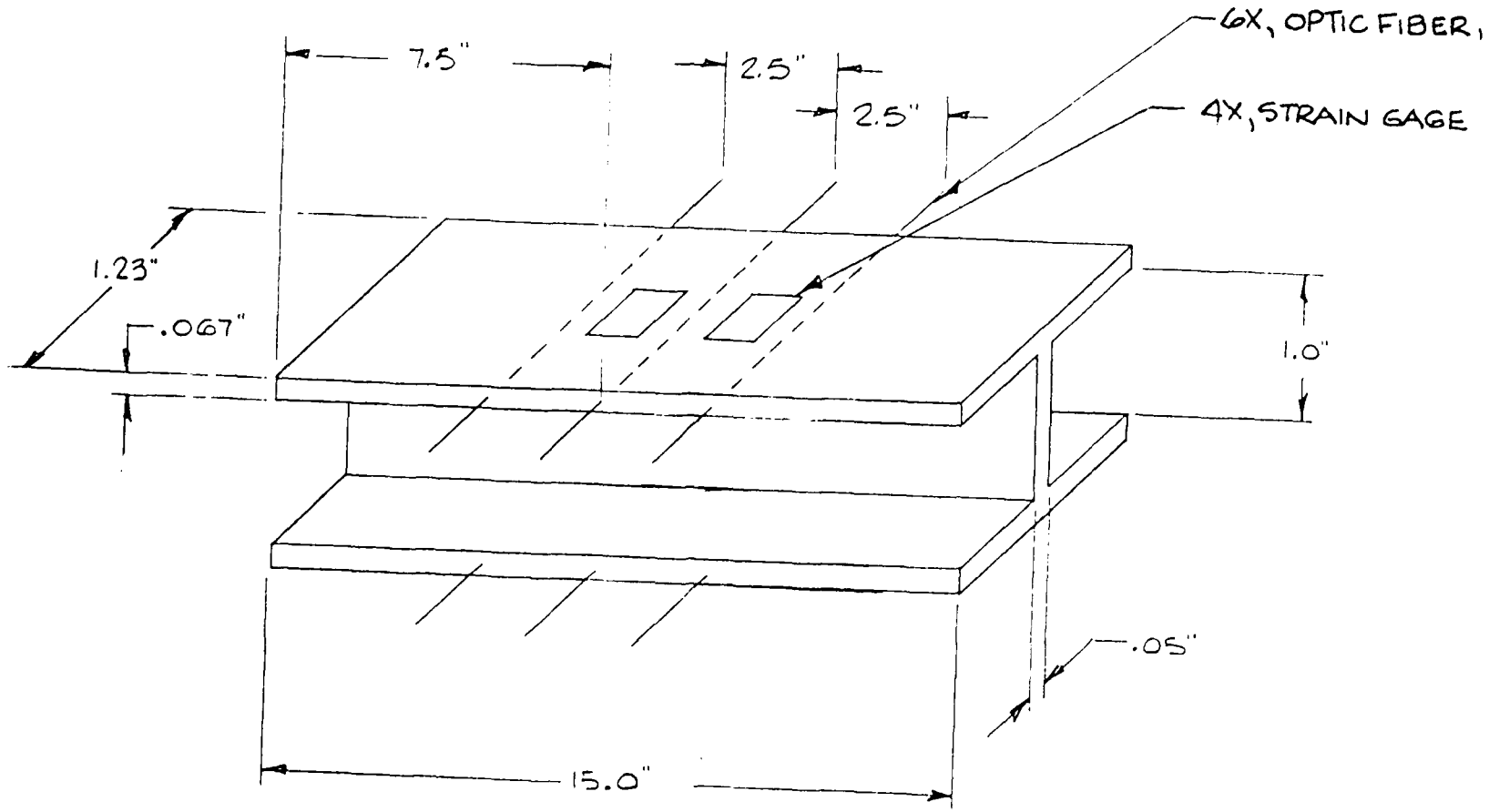

FIGURE 17. I-BEAM DIMENSIONS

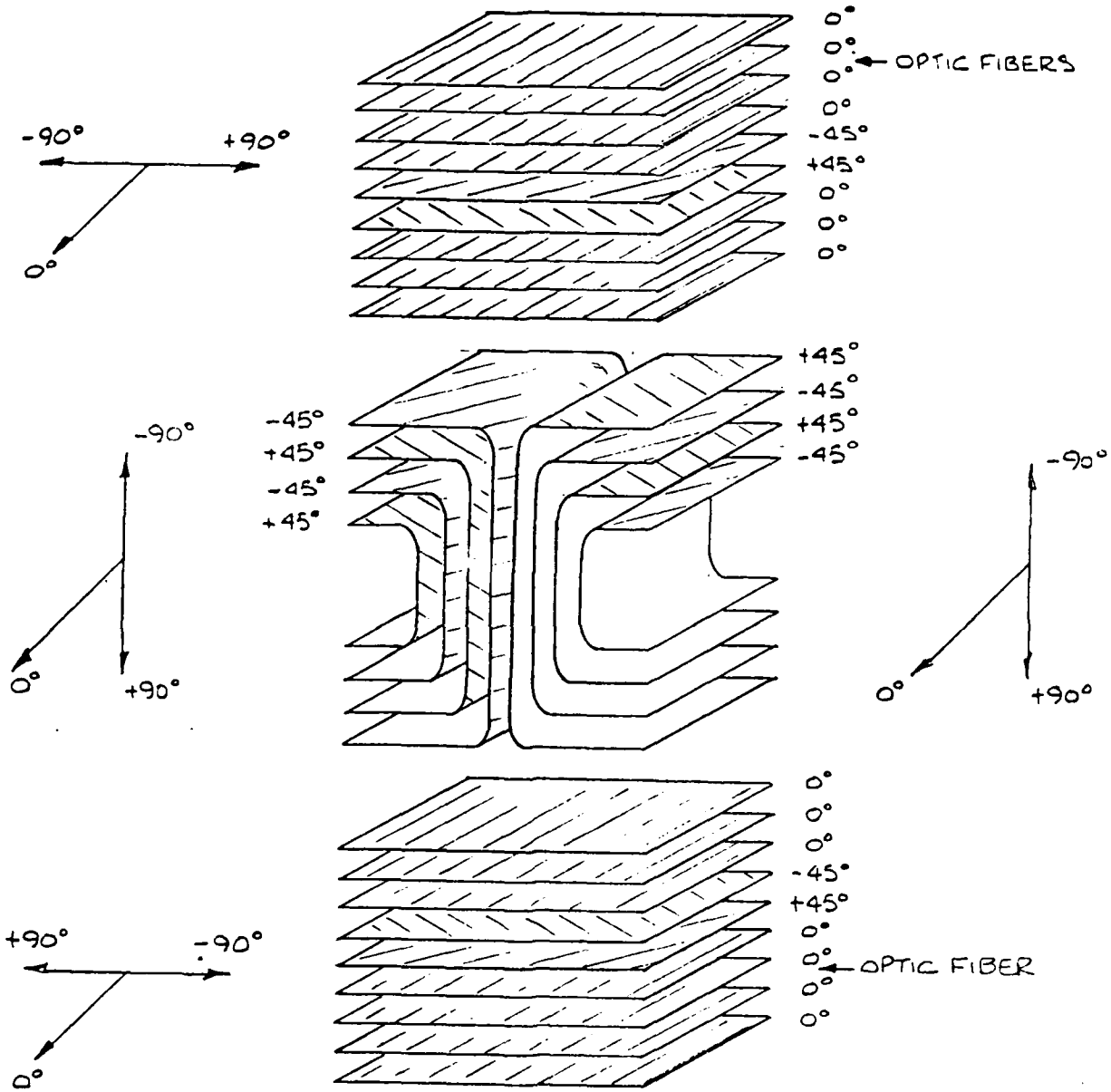

FIGURE 18. I-BEAM LAY UP

FIGURE 19 . FULLY INSTRUMENTED I-BEAM PHOTOGRAPH

TABLE 10. I-BEAM OPTICAL FIBER SURVIVAL RATE

	LEFT	CENTER	RIGHT
I-BEAM #1			
Top Flange	F	P	F*
Bottom Flange	P	F	F*
I-BEAM #2			
Top Flange	F*	F	P
Bottom Flange	P*	P	P

Bare Fiber Survival Rate = 5/8 = 63%

Gold Fiber Survival Rate = 1/4 = 25%

Overall Survival Rate = 6/12 = 50%

P = Passed Optical Continuity Test

F = Failed Optical Continuity Test

*Gold Fiber

location. One half of the optical fibers embedded survived. The bare fiber survival rate was 63% while the gold fiber survival rate was 25%.

3.3 I-Beam Four Point Bend Test

Four point bend testing was performed on the two I-beams. Figure 20 shows the I-beam in the four point bend fixture while Figure 21 shows an overview of the entire system.

Beam #1 had the center fiber on the top flange tested with the six measurements outlined in Section 2.2. Data from measurement #1 is shown in Figure 22. Data reduction is the same as described in Section 2.2 and reduced data is listed in Table 11. Left and right optical fibers were referenced to left and right resistive strain gages, respectively. Center optical fibers were referenced to the average of left and right strain gages. Figure 23 shows a plot of the reduced data (loading only) for measurement #1. Optical output and resistive output clearly correspond in a linear manner.

Table 11 also contains reduced data for the other surviving optical fibers. System repeatability can be determined to be $\pm$2% from I-beam #1 center fiber results.

Fiber to fiber repeatability was determined to be $\pm$15% when all the surviving fibers were considered. Factors believed to be responsible for the variation are listed below:

- Embedded length
- Composite elastic constants
- Optical fiber elastic constants
- Optical fiber photoelastic constants

In any event sensor to sensor variations this large would require calibration after embedment. Reduction of this variation should be considered a subject for future work.

Gold coated fiber raw data is presented in Figure 24 and the reduced data is shown in Figure 25. Hysteresis is present for this fiber and the optical signal did not return to its starting point, unlike the resistive strain gage or the uncoated optical fiber.

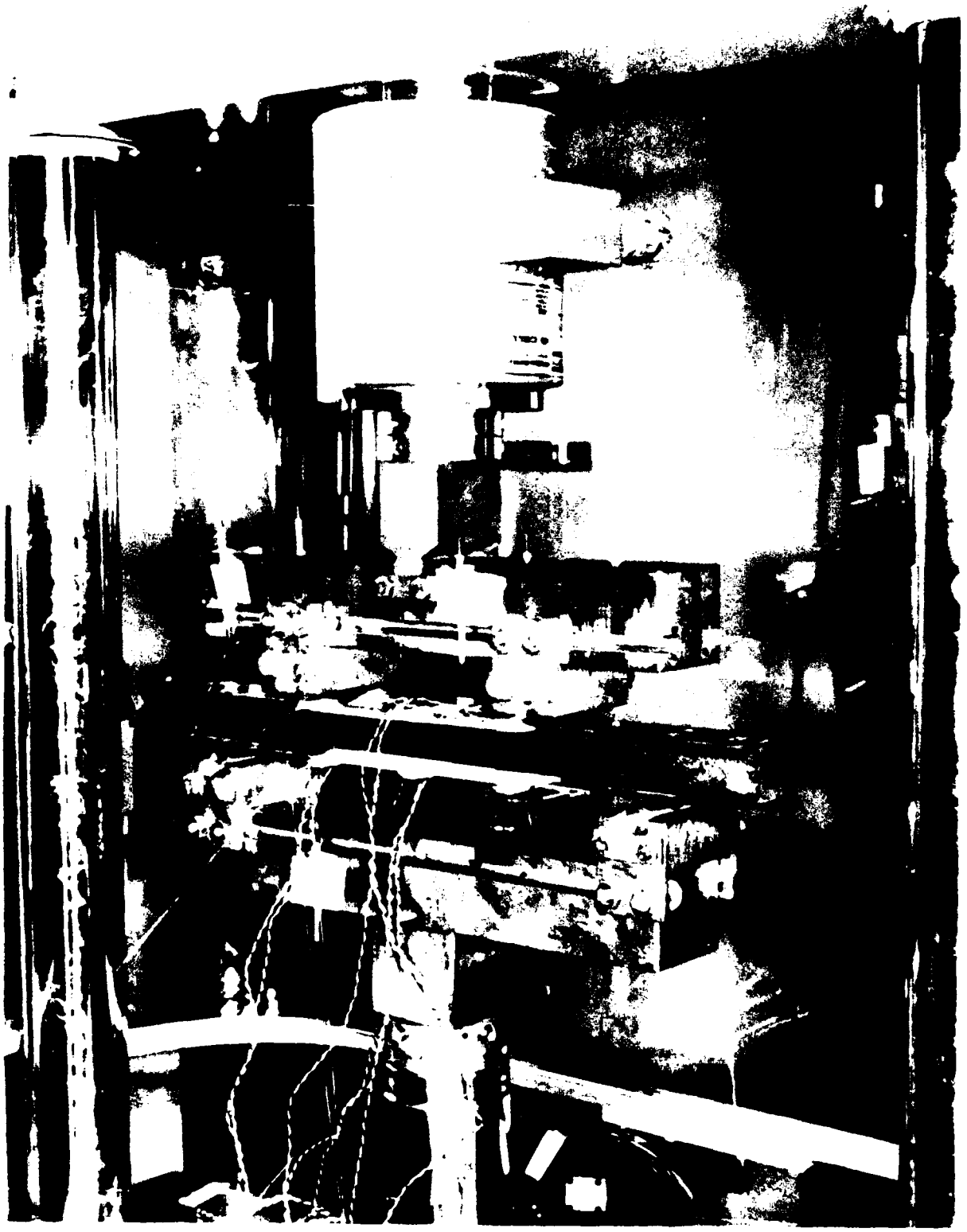

FIGURE 20 . I-BEAM FOUR POINT LOADING FIXTURE PHOTOGRAPH

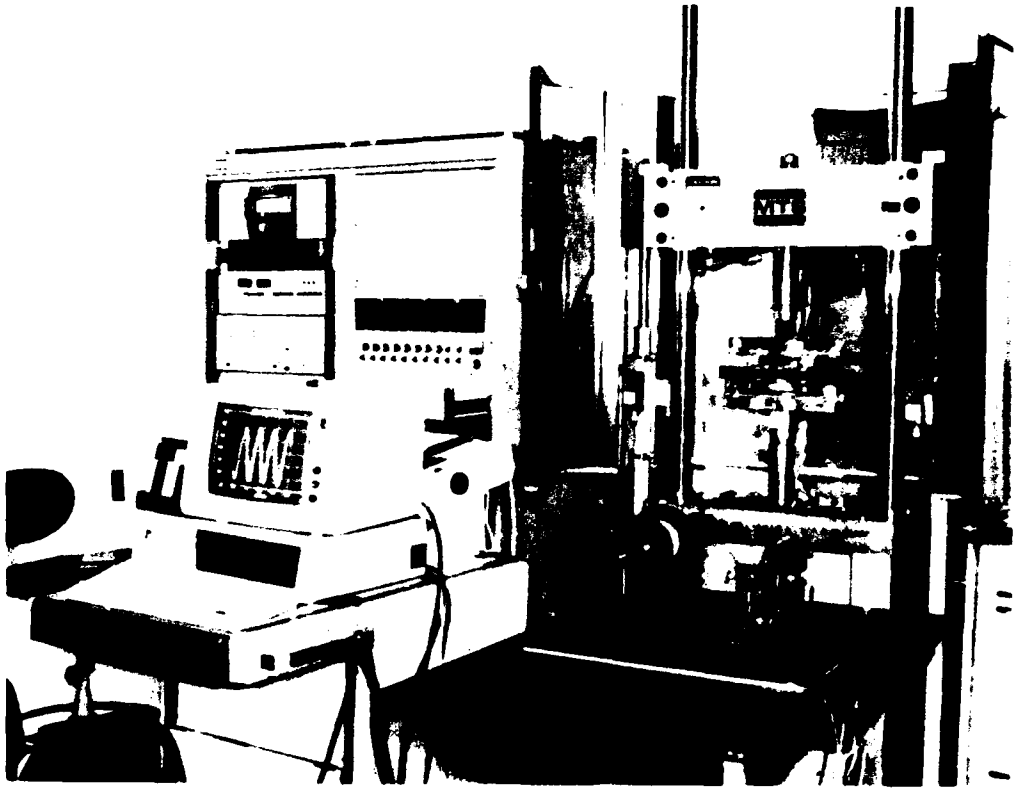

FIGURE 21 . I-BEAM MEASUREMENT EQUIPMENT PHOTOGRAPH

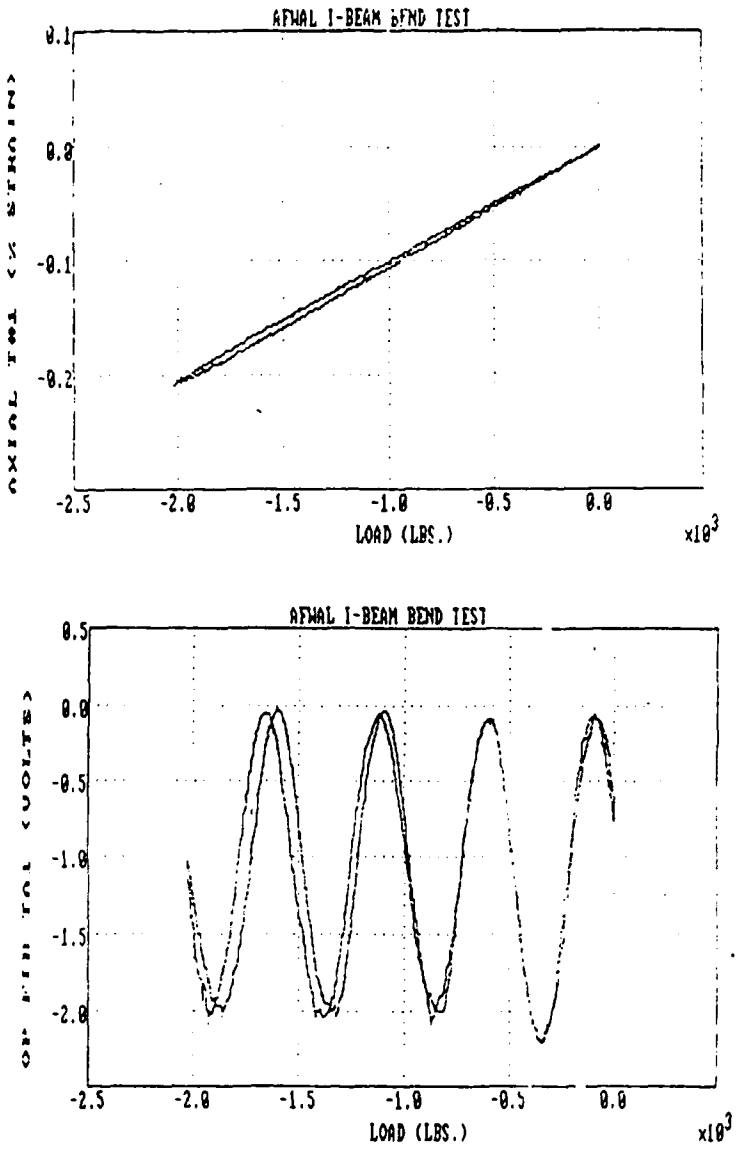

FIGURE 22. I-BEAM DATA PLOT

TABLE 11 . I-BEAM OPTICAL RESPONSIVITY FRINGES/ % ε • IN

	LEFT	CENTER	RIGHT
BEAM #1			
TOP	F	17.75, 17.75, 18.17 18.03, 17.97, 18.52	F*
BOTTOM	19.59	F	F*
BEAM #2			
TOP	F*	F	15.06
BOTTOM	16.38*	20.27	15.58

F = Failed Optical Continuity Test

* = Gold Fiber Results @ 632 scaled to 820 nm

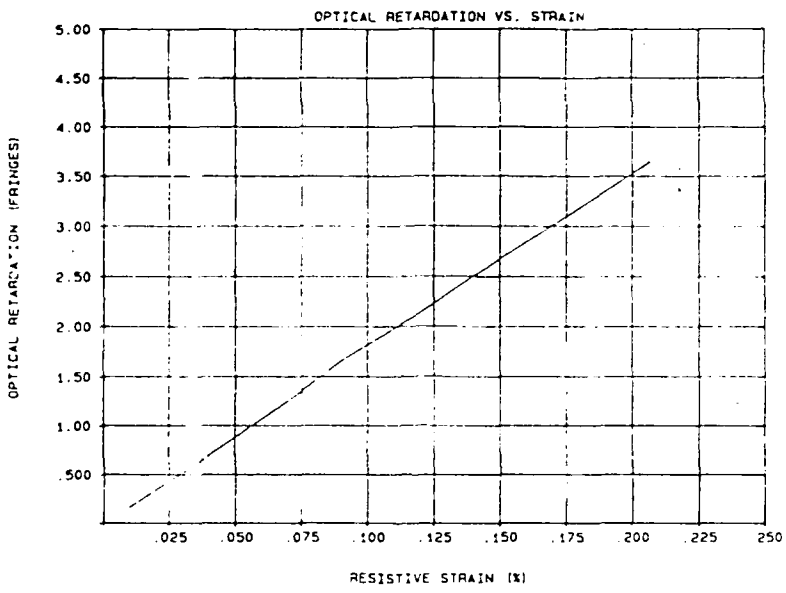

FIGURE 23. I-BEAM REDUCED DATA PLOT

(Loading Only)

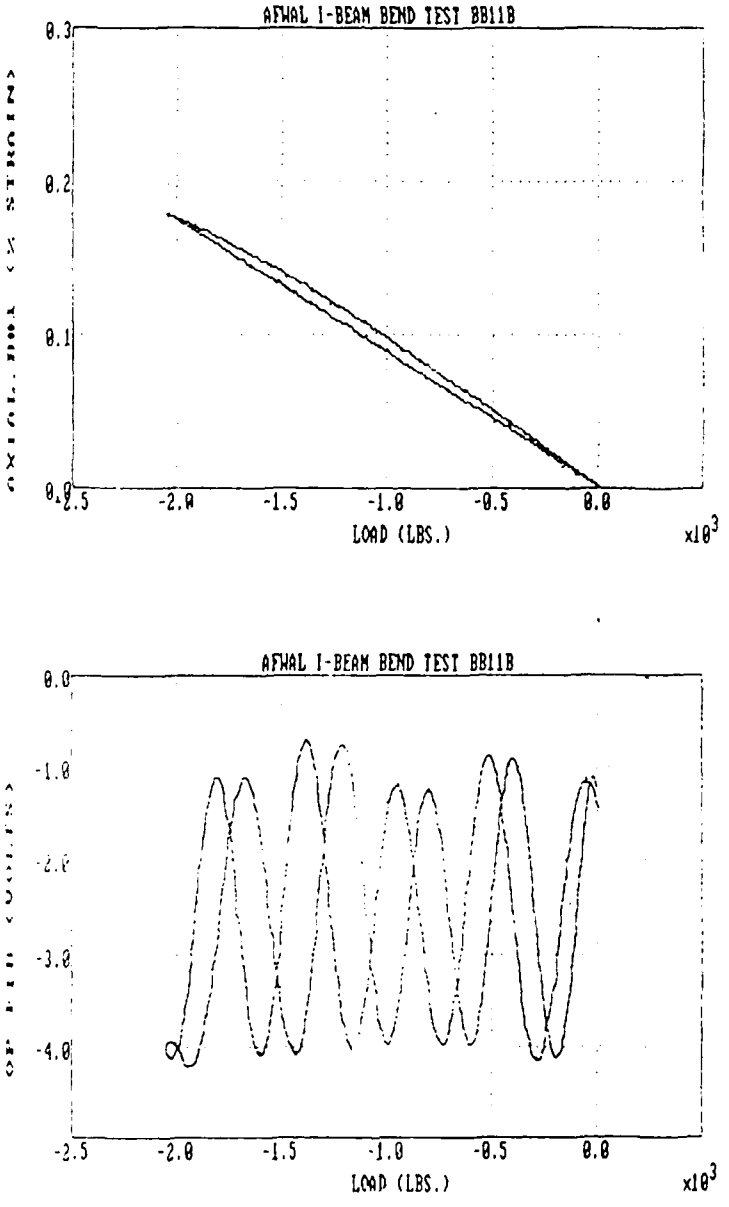

FIGURE 24 . GOLD FIBER DATA PLOT

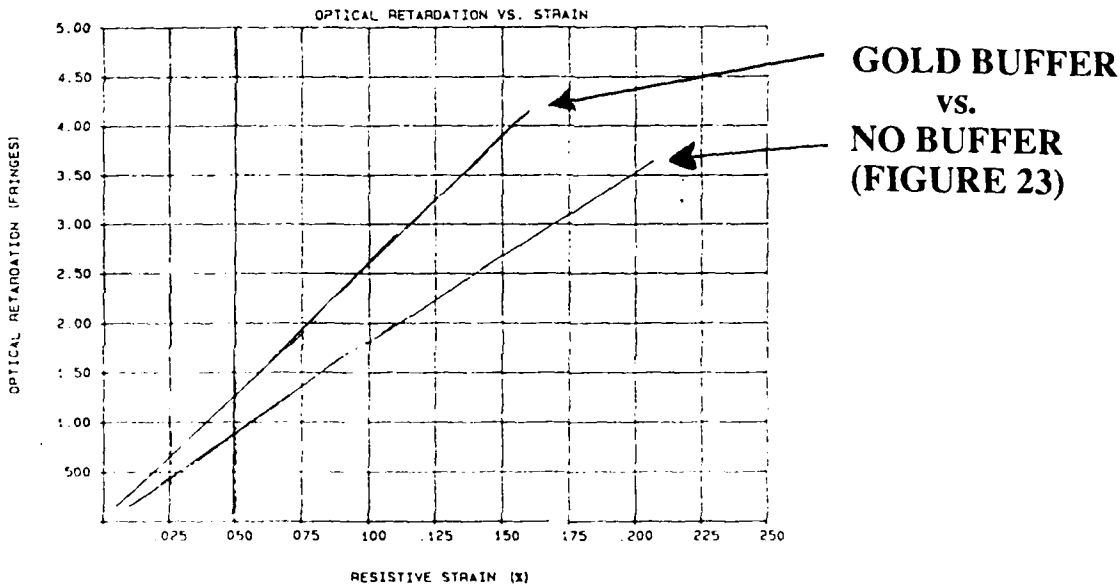

FIGURE 25. GOLD FIBER REDUCED DATA PLOT

Optical responsivity for the gold fiber was higher than the bare fiber of Figure 23 as shown in Figure 25. The gold coated fiber had an operating wavelength of 632.8 nm while the bare fiber used operates at 820 nm.

Identical retardations will result in larger phase shifts when a shorter wavelength is used. Optical responsivity of the gold fiber is scaled downward by 632.8/820 in Table 11. Results can be compared on an equal basis.

3.4 I-Beam Load to Failure Test

One of the two I-beams fabricated for the four point bend tests was loaded to failure using the identical fixturing. Failure occurred at 2660 lbs. due to web shear buckling occurring in the upper portion (compression side) of the web under one of the roller supports as shown in Figure 26. A comparison of the actual and predicted failure loads is shown in Table 12.

An analysis of the beam was performed to predict the failure load and mode of failure. Compressive and tensile strengths for the flanges were calculated using a progressive failure analysis with a modified maximum strain failure criteria. The following strain allowables were used:

$$\varepsilon_{11T} = 1.51\ \%$$
$$\varepsilon_{12T} = 0.58\%$$
$$\varepsilon_{12} = 2.54\%$$
$$\varepsilon_{11C} = -1.09\%$$
$$\varepsilon_{22C} = -2.78\%$$

From these stain allowables the following flange strengths were calculated:

τ_C	=	72.6 ksi	Compressive Strength
τ_r	=	81.4 ksi	Tensile Strength
τ_b	=	32.8 ksi	Buckling Strength

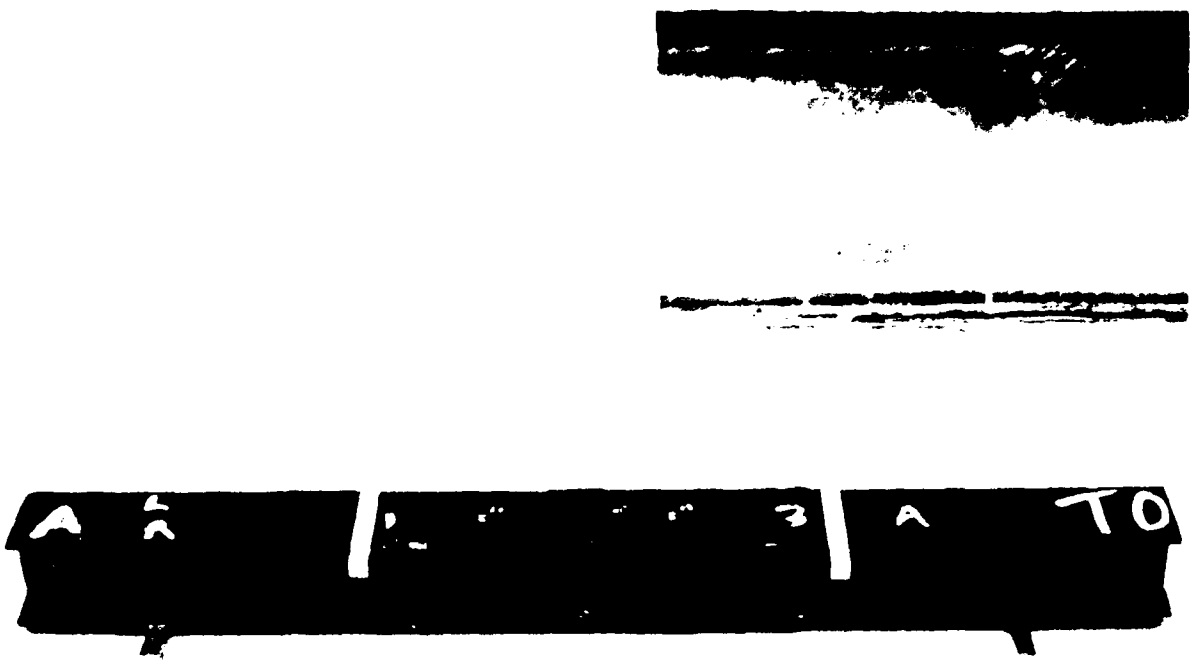

FIGURE 26. FAILED I-BEAM

TABLE 12. PREDICTED VS. ACTUAL I-BEAM FAILURE LOADS

	ACTUAL	PREDICTED
LOAD	2660 Lbs.	3082 Lbs.
FAILURE MODE	Web Shear Buckling	Flange Compressive Buckling

Maximum bending stress occurs at the mid-point of the beam, therefore failure was predicted to occur due to compressive buckling of the flange at the beam mid-point. The buckling failure load is calculated as follows:

$$2P = \frac{\tau_c}{2.5\,c} = 3082 \text{ lbs.}$$

Failure due to shear buckling in the web was also considered. The maximum shear stress occurs at the ends of the beam. The shear stress was predicted as follows:

$$\tau_{cr} = 49{,}357 \text{ psi}$$

The calculated shear load to cause buckling was then calculated to be:

$$2P - \tau_{cr}A = 4304 \text{ lbs.}$$

This load was greater than the load necessary to buckle the flange and therefore was predicted not to be the dominate failure mode.

The analysis predicted failure due to buckling of the compressive flange at a load of 3082 lbs. Although the magnitudes of the actual and the predicted failure loads compared very well (Table 12), there was a discrepancy in the mode of failure. The analysis predicted failure due to flange buckling at the beam mid-point whereas the actual failure occurred in the web due to shear buckling. The fact that the analysis did not take into account the non-linear shear stress distribution in the web nor the stress concentrations in the area of the roller supports is a possible explanation for this discrepancy.

3.5 I-Beam Test Analysis

Section 3.3 presented optical responsivity correlated to a resistive strain gage mounted on the beam surface. Analysis developed in Section 2.6 modeled optical retardation correlated to strain applied to the optical fiber. Strain at the optical fiber is related to strain at the beam surface by the ratio of distances from the neutral axis:

$$\frac{\varepsilon_{to}}{\varepsilon_{cm}} = \frac{x}{t}$$

(3.5-1)

where:

ε_{to}	=	transverse strain at the optical fiber plane
ε_m	=	measured strain at beam surface
t	=	beam half height
x	=	distance from beam neutral axis to optical fiber plane

For the beam under consideration, the ratio x/t is .98. Sensor responsivity correlated to resistive strain can be converted to responsivity at the fiber plane via the equation:

$$n_{to} = n_{tm} \frac{\varepsilon_{tm}}{\varepsilon_{t0}}$$

(3.5-2)

Table 13 contains the converted responsivity data. Optical responsivity is 17.86 fringe/% ε • in with a standard deviation of 2.2 fringe/% ε •in. Coupon test data shows a fiber responsivity of 17.09 fringe/% ε • in. With a standard deviation of 2.7 fringe/% ε • in. These numbers are identical given the variance in the data.

TABLE 13. I-BEAM FIBER OPTICAL RESPONSIVITY FRINGE/% ε • IN

	LEFT	CENTER	RIGHT
I-BEAM #1			
TOP FLANGE	N/A	18.42	N/A
BOTTOM FLANGE	20.01	N/A	N/A
I-BEAM #2			
TOP FLANGE	N/A	15.39	N/A
BOTTOM FLANGE	16.73	20.71	15.92

FIBER AVERAGE = 17.86 $\frac{\text{FRINGE}}{\%\varepsilon \cdot \text{in}}$

STANDARD DEV. = 2.2 $\frac{\text{FRINGE}}{\%\varepsilon \cdot \text{in}}$

4.0 CONCLUSIONS

Strain measurement using the polarimetric technique combined with low birefringence fiber was successful in measuring strain applied transversely to optic fiber axis. The technique was demonstrated in composite coupons with two loading configurations and in a composite I-beam in four point bending with resistive strain gages as a reference.

Strain measurement using the polarimetric technique combined with high birefringence fiber was not successful in measuring strain applied parallel to the optic fiber axis. The sensor was found to have a relatively large sensitivity to strain applied normal to the optic fiber axis. Measurement was further complicated by laser diode wavelength fluctuations with temperature. Therefore, high birefringence fibers were not embedded in the I-beam.

Optical time domain reflectometry was used to locate point loads within composite coupons. Demonstrated instrumentation spatial resolution was 1.2 meters. OTDR sensor embedded in composite coupons shows no response until 64 Ksi compressive stress was applied. High stress levels indicate that a suitable application of OTDR technology is damage detection. It should be noted that acrylate buffers were in place during OTDR testing and specialty coatings may improve the signal detection level.

Optic fiber survival rate was about 50% during the two fabrication phases of the contract. Specialty coatings will be required to protect the fibers during fabrication and provide good mechanical transfer of load.

5.0 RECOMMENDATIONS

The recommendations for further work are:

1. To investigate and improve the embedded fiber optic sensor survivability during manufacture of a composite structure. The recommendation is to investigate various fiber optic coatings that would protect the optic fiber and would be compatible with the composite matrix while at the same time would not exhibit any undesirable hysteresis effects.

2. To investigate and improve the embedded polarimetric strain sensor and measurement technique.

    a. In the areas of sensor to sensor repeatability.
    b. To enable it to perform absolute measurements.
    c. Since the fiber optic sensor has the potential to sense the direction a load is being applied, as well as its magnitude (unlike a resistive strain gauge that senses only in one direction). It is recommended that this ability be investigated and characterized.

3. Improve the composite Damage Detection Techniques using OTDR or a variation of it to characterize damage types (Hard/Soft) and measurement/detection levels.

4. Investigate composite strain measurement techniques using polarimetric and/or combined reflectometry techniques to determine an approach that can extend the measurement approach from a point sensing system to one that can make distributed strain measurements.

REFERENCES

1. Rashleight; S.C.; Origins and Control of Polarization Effects in Single-Mode Fibers; Journal of Lightwave Technology; Vol. LT-1, No. 2, June 1983 Pages 312-331.

2. Jeglinski, S.A.; Brennan, B. W. ; Spillman, W.B.; Lord, J.R.; Comparison of Fiber Optic and Resistive Strain Gage Techniques foir Composite Monitoring Applications; Proceedings of the 33rd International Instrumentation Symposium, May 3 - 8 1987, Instrument Soiciety of America; Pages 283-291.

3. Theocaris, P.S.; Gdoutos, E.E.; Matrix Theory of Photoelasticity; Springer-Verlag Berlin, Heidleberg, 1979.

4. Namihira;, Y, Opto-Elastic constant in Single Mode Optical Fibers; Journal of Lightwave Technology; Vol. LT-3, No. 5 October, 1985; Pages 1078-1083.

5. Timoshenko, S.P.; Goodier, J.N.; "Theory of Elasticity", 1970 McGraw-Hill Inc., Page 167.

6. Mermelstein, M.D., "High-Birefringence Fiber Optic Polarimeter with Submicroradian Phase Delay Detectability, "Journal of Lightwave Technology, LT-4, pages. 479-453. April, 1986.

APPENDICES

A. STATEMENT OF WORK

1. PRELIMINARY FABRICATION AND TESTING

1.1 Planning and scheduling meeting with all principal parties. Establish and submit program schedule, IAW data item CLIN 0001, items 2 and 3.

1.2 Fabricate the following uniaxial, graphite/epoxy coupons (3 of each) of standard dimension:

a. tensile with optical fibers aligned longitudinally and placed at the neutral axis.
b. same as a., but with fibers half way between the neutral axis and the surface.
c. same as b., but with optical fibers aligned perpendicular to the graphite fiber axis.
d. same as a., but a compressive specimen.

In each case there will be three different optical fibers embedded, 850 step index single mode, 850 polarization preserving, and 50/125 multimode.

e. same as a., but without optical fibers.
f. same as d., but without optical fibers.

note: all coupons to be cured in the same autoclave cycle to prevent processing variabilities.

1.3 Perform three or four point bending tests on specimens a.-c. (this will be determined by the availability of existing fixturing). Monitor strain with the optical sensors using the polarimetric technique and OTDR when appropriate. Also monitor the strain with surface attached resistive strain gauges.

1.4 Perform compression tests on specimens d. while making the same measurements as in 1.3.

1.5 Stress to failure all specimens (a.-e.) and compare their ultimate strength with expected results.

1.6 Analyze the results from the above experiments and compare them with theory previously developed.

1.7 Presentation of preliminary results to Project Management at WPAFB. Prepare and present IAW CLIN 0001, item 4.

2. I-BEAM STRUCTURAL FABRICATION AND TESTING

2.1 Fabricate an I-beam with the same optical fibers described above placed in both caps and in the web.

2.2 Perform three or four point bending tests (depending on the availability of fixturing). Monitoring the strain with the optical sensors as in paragraph 1.3.

2.3 Stress I-beam to failure and compare ultimate strain to expected strain.

2.4 Analyze these results and compare with performance expected from task 1.

2.5 Prepare final report and present results to Project Management at WPAFB, IAW CLIN 0001, item 5.

*U.S.Government Printing Office: 1990 - 748-056/24285